Determination of α_s in second order QCD from hadronic Z decays

P. Abreu, W. Adam, F. Adami, T. Adye, T. Akesson, G.D. Alekseev, P. Allen, S. Almehed, S.J. Alvsvaag, U. Amaldi, et al.

EUROPEAN ORGANIZATION FOR NUCLEAR RESEARCH

Determination of α_S in Second Order QCD in Hadronic Z Decays

DELPHI Collaboration

Abstract

Distributions of event shape variables obtained from 120600 hadronic Z decays measured with the DELPHI detector are compared to the predictions of QCD based event generators. Values of the strong coupling constant α_s are derived as a function of the renormalization scale from a quantitative analysis of eight hadronic distributions. The final result, $\alpha_s(M_Z) = 0.113 \pm 0.007$, is based on second order perturbation theory and uses two hadronization corrections, one computed with a parton shower model and the other with a QCD matrix element model.

P.Abreu[18], W.Adam[43], F.Adami[34], T.Adye[32], T.Akesson[21], G.D.Alu.seev[13], P.Allen[42], S.Almehed[21],
S.J.Alvsvaag[4], U.Amaldi[7], E.G.Anassontsis[3], P.Antilogus[22], W-D.Apel[14], R.J.Apsimon[32], B.Åsman[38],
J-E.Augustin[16], A.Augustinus[27], P.Baillon[7], P.Bambade[16], F.Barao[18], R.Barate[11], G.Barbiellini[40],
D.Y.Bardin[13], A.Baroncelli[35], O.Barring[21], W.Bartl[43], M.J.Bates[30], M.Battaglia[25], M.Baubillier[20],
K-H.Becks[45], C.J.Beeston[30], M.Begalli[10], P.Beilliere[6], Yu.Belokopytov[37], K.Belous[37], P.Beltran[9], D.Benedic[8],
J.M.Benlloch[42], M.Berggren[16], D.Bertrand[2], F.Bianchi[39], M.S.Bilenky[13], P.Billoir[20], J.Bjarne[21], D.Bloch[8],
S.Blyth[30], V.Bocci[33], P.N.Bogolubov[13], T.Bolognese[34], M.Bonapart[27], M.Bonesini[25], W.Bonivento[25],
P.S.L.Booth[19], P.Borgeaud[34], G.Borisov[37], H.Borner[7], C.Bosio[35], B.Bostjancic[7], O.Botner[41], B.Bouquet[16],
C.Bourdarios[16], T.J.V.Bowcock[19], M.Bozzo[10], S.Braibant[2], P.Branchini[35], K.D.Brand[31], R.A.Brenner[12],
H.Briand[20], C.Bricman[2], R.C.A.Brown[7], N.Brummer[27], J-M.Brunet[6], L.Bugge[29], T.Buran[29], H.Burmeister[7],
J.A.M.A.Buytaert[7], M.Caccia[7], M.Calvi[25], A.J.Camacho Rozas[36], T.Camporesi[7], V.Canale[33], F.Cao[2],
F.Carena[7], L.Carroll[19], C.Caso[10], E.Castelli[40], M.V.Castillo Gimenez[42], A.Cattai[7], F.R.Cavallo[5], L.Cerrito[33],
A.Chan[1], M.Chapkin[37], P.Charpentier[7], L.Chaussard[16], J.Chauveau[20], P.Checchia[31], G.A.Chelkov[13],
L.Chevalier[34], P.Chliapnikov[37], V.Chorowicz[20], R.Cirio[39], M.P.Clara[39], P.Collins[30], J.L.Contreras[23],
R.Contri[10], G.Cosme[16], F.Couchot[16], H.B.Crawley[1], D.Crennell[32], G.Crosetti[10], M.Crozon[6],
J.Cuevas Maestro[36], S.Czellar[12], S.Dagoret[16], E.Dahl-Jensen[26], B.Dalmagne[16], M.Dam[29], G.Damgaard[26],
G.Darbo[10], E.Daubie[2], P.D.Dauncey[30], M.Davenport[7], P.David[20], W.Da Silva[20], C.Defoix[6], D.Delikaris[7],
S.Delorme[7], P.Delpierre[6], N.Demaria[39], A.De Angelis[40], M.De Beer[34], H.De Boeck[2], W.De Boer[14],
C.De Clercq[2], M.D.M.De Fez Laso[42], N.De Groot[27], C.De La Vaissiere[20], B.De Lotto[40], A.De Min[25],
H.Dijkstra[7], L.Di Ciaccio[33], F.Djama[8], J.Dolbeau[6], M.Donszelmann[27], K.Doroba[44], M.Dracos[7], J.Drees[45],
M.Dris[28], Y.Dufour[6], W.Dulinski[8], R.Dzhelyadin[37], L-O.Eek[41], P.A.-M.Eerola[7], T.Ekelof[41], G.Ekspong[38],
A.Elliot Peisert[31], J-P.Engel[8], D.Fassouliotis[28], M.Feindt[7], A.Fenyuk[37], M.Fernandez Alonso[36], A.Ferrer[42],
T.A.Filippas[28], A.Firestone[1], H.Foeth[7], E.Fokitis[28], P.Folegati[40], F.Fontanelli[10], K.A.J.Forbes[19], B.Franek[32],
P.Frenkiel[6], D.C.Fries[14], A.G.Frodesen[4], R.Fruhwirth[43], F.Fulda-Quenzer[16], K.Furnival[19], H.Furstenau[14],
J.Fuster[7], G.Galeazzi[31], D.Gamba[39], C.Garcia[42], J.Garcia[36], C.Gaspar[7], U.Gasparini[31], P.Gavillet[7],
E.N.Gazis[28], J-P.Gerber[8], P.Giacomelli[7], R.Gokieli[7], V.M.Golovatyuk[13], J.J.Gomes Y Cadenas[7], A.Goobar[38],
G.Gopal[32], M.Gorski[44], V.Gracco[10], A.Grant[7], F.Grard[2], E.Graziani[35], G.Grosdidier[16], E.Gross[7],
P.Grosse-Wiesmann[7], B.Grossetete[20], J.Guy[32], F.Hahn[7], M.Hahn[14], S.Haider[27], Z.Hajduk[15], A.Hakansson[21],
A.Hallgren[41], K.Hamacher[45], G.Hamel De Monchenault[34], F.J.Harris[30], B.W.Heck[7], T.Henkes[7],
J.J.Hernandez[42], P.Herquet[2], H.Herr[7], T.L.Hessing[19], I.Hietanen[12], C.O.Higgins[19], E.Higon[42], H.J.Hilke[7],
S.D.Hodgson[30], T.Hofmokl[44], R.Holmes[1], S-O.Holmgren[38], D.Holthuizen[27], P.F.Honore[6], J.E.Hooper[26],
M.Houlden[19], J.Hrubec[43], P.O.Hulth[38], K.Hultqvist[38], D.Husson[8], P.Ioannou[3], D.Isenhower[7], P-S.Iversen[4],
J.N.Jackson[19], P.Jalocha[15], G.Jarlskog[21], P.Jarry[34], B.Jean-Marie[16], E.K.Johansson[38], D.Johnson[19],
M.Jonker[7], L.Jonsson[21], P.Juillot[8], G.Kalkanis[3], G.Kalmus[32], F.Kapusta[20], M.Karlsson[7], A.Katargin[37],
S.Katsanevas[3], E.C.Katsoufis[28], R.Keranen[12], J.Kesteman[2], B.A.Khomenko[13], N.N.Khovanski[13], B.King[19],
N.J.Kjaer[7], H.Klein[7], W.Klempt[7], A.Klovning[4], P.Kluit[27], J.H.Koehne[14], B.Koene[27], P.Kokkinias[9], M.Kopf[14],
M.Koratzinos[39], K.Korcyl[15], A.V.Korytov[13], V.Kostioukhine[37], C.Kourkoumelis[3], P.H.Kramer[45],
T.Kreuzberger[43], J.Krolikowski[44], I.Kronkvist[21], J.Krstic[30], U.Kruener-Marquis[45], W.Krupinski[15],
W.Kucewicz[25], K.Kurvinen[12], C.Lacasta[42], C.Lambropoulos[9], J.W.Lamsa[1], L.Lanceri[40], V.Lapin[37],
J-P.Laugier[34], R.Lauhakangas[12], G.Leder[43], F.Ledroit[11], R.Leitner[7], Y.Lemoigne[34], J.Lemonne[2], G.Lenzen[45],
V.Lepeltier[16], A.Letessier-Selvon[20], E.Lieb[45], D.Liko[43], E.Lillethun[4], J.Lindgren[12], R.Lindner[45], A.Lipniacka[44],
I.Lippi[31], R.Llosa[23], B.Loerstad[21], M.Lokajicek[13], J.G.Loken[30], A.Lopez-Fernandez[16], M.A.Lopes Aguera[36],
M.Los[27], D.Loukas[9], A.Lounis[8], J.J.Lozano[42], P.Lutz[6], L.Lyons[30], G.Maehlum[7], J.Maillard[6], A.Maltezos[9],
F.Mandl[43], J.Marco[36], M.Margoni[31], J-C.Marin[7], A.Markou[9], T.Maron[45], S.Marti[42], L.Mathis[1], F.Matorras[36],
C.Matteuzzi[25], G.Matthiae[33], M.Mazzucato[31], M.Mc Cubbin[19], R.Mc Kay[1], R.Mc Nulty[19], E.Menichetti[39],
G.Meola[10], C.Meroni[25], W.T.Meyer[1], M.Michelotto[31], W.A.Mitaroff[43], G.V.Mitselmakher[13], U.Mjoernmark[21],
T.Moa[38], R.Moeller[26], K.Moenig[7], M.R.Monge[10], P.Morettini[10], H.Mueller[14], W.J.Murray[32], B.Muryn[16],
G.Myatt[30], F.Naraghi[20], F.L.Navarria[5], P.Negri[25], B.S.Nielsen[26], B.Nijjhar[19], V.Nikolaenko[37], V.Obraztsov[37],
K.Oesterberg[12], A.G.Olshevski[13], R.Orava[12], A.Ostankov[37], A.Ouraou[34], M.Paganoni[25], R.Pain[20], H.Palka[27],
T.Papadopoulou[28], L.Pape[7], A.Passeri[35], M.Pegoraro[31], J.Pennanen[12], V.Perevozchikov[37], M.Pernicka[43],
A.Perrotta[5], F.Pierre[34], M.Pimenta[18], O.Pingot[2], M.E.Pol[7], G.Polok[15], P.Poropat[40], P.Privitera[14], A.Pullia[25],
D.Radojicic[30], S.Ragazzi[25], P.N.Ratoff[17], A.L.Read[29], N.G.Redaelli[25], M.Regler[43], D.Reid[19], P.B.Renton[30],
L.K.Resvanis[3], F.Richard[16], M.Richardson[19], J.Ridky[13], G.Rinaudo[39], I.Roditi[7], A.Romero[39], I.Roncagliolo[10],
P.Ronchese[31], V.Ronjin[37], C.Ronnqvist[12], E.I.Rosenberg[1], U.Rossi[5], E.Rosso[7], P.Roudeau[16], T.Rovelli[5],
W.Ruckstuhl[27], V.Ruhlmann[34], A.Ruiz[36], K.Rybicki[15], H.Saarikko[12], Y.Sacquin[34], G.Sajot[11], J.Salt[42],
E.Sanchez[42], J.Sanchez[23], M.Sannino[10], M.Schaeffer[8], S.Schael[14], H.Schneider[14], M.A.E.Schyns[45], F.Scuri[40],
A.M.Segar[30], R.Sekulin[32], M.Sessa[40], G.Sette[10], R.Seufert[14], R.C.Shellard[7], P.Siegrist[34], S.Simonetti[10],
F.Simonetto[31], A.N.Sissakian[13], T.B.Skaali[29], G.Skjevling[29], G.Smadja[34,22], N.Smirnov[37], G.R.Smith[32],

R.Sosnowski[44], T.S.Spassoff[11], E.Spiriti[35], S.Squarcia[10], H.Staeck[45], C.Stanescu[35], G.Stavropoulos[9], F.Stichelbaut[2], A.Stocchi[16], J.Strauss[43], J.Straver[7], R.Strub[8], M.Szczekowski[44], M.Szeptycka[44], P.Szymanski[44], T.Tabarelli[25], S.Tavernier[2], O.Tchikilev[37], G.E.Theodosiou[9], A.Tilquin[24], J.Timmermans[27], V.G.Timofeev[13], L.G.Tkatchev[13], T.Todorov[13], D.Z.Toet[27], O.Toker[12], A.Tomaradze[37], E.Torassa[39], L.Tortora[35], M.T.Trainor[30], D.Treille[7], U.Trevisan[10], W.Trischuk[7], G.Tristram[6], C.Troncon[25], A.Tsirou[7], E.N.Tsyganov[13], M.Turala[15], R.Turchetta[8], M-L.Turluer[34], T.Tuuva[12], I.A.Tyapkin[13], M.Tyndel[32], S.Tsamarias[7], S.Ueberschaer[45], O.Ullaland[7], V.Uvarov[37], G.Valenti[5], E.Vallazza[39], J.A.Valls Ferrer[42], C.Vander Velde[2], G.W.Van Apeldoorn[27], P.Van Dam[27], W.K.Van Doninck[2], J.Varela[18], P.Vaz[7], G.Vegni[25], L.Ventura[31], W.Venus[32], F.Verbeure[2], L.S.Vertogradov[13], D.Vilanova[34], N.Vishnevsky[37], L.Vitale[40], E.Vlasov[37], S.Vlassopoulos[28], A.S.Vodopyanov[13], M.Vollmer[45], S.Volponi[5], G.Voulgaris[3], M.Voutilainen[12], V.Vrba[35], H.Wahlen[45], C.Walck[38], F.Waldner[40], M.Wayne[1], A.Wehr[45], M.Weierstall[45], P.Weilhammer[7], J.Werner[45], A.M.Wetherell[7], J.H.Wickens[2], J.Wikne[29], G.R.Wilkinson[30], W.S.C.Williams[30], M.Winter[8], D.Wormald[29], G.Wormser[16], K.Woschnagg[41], N.Yamdagni[38], P.Yepes[7], A.Zaitsev[37], A.Zalewska[15], P.Zalewski[16], D.Zavrtanik[7], E.Zevgolatakos[9], G.Zhang[45], N.I.Zimin[13], M.Zito[34], R.Zitoun[20], R.Zukanovich Funchal[6], G.Zumerle[31], J.Zuniga[42]

[1] Ames Laboratory and Department of Physics, Iowa State University, Ames IA 50011, USA
[2] Physics Department, Univ. Instelling Antwerpen, Universiteitsplein 1, B-2610 Wilrijk, Belgium
   and IIHE, ULB-VUB, Pleinlaan 2, B-1050 Brussels, Belgium
   and Service de Phys. des Part. Elém., Faculté des Sciences, Université de l'Etat Mons, Av. Maistriau 19, B-7000 Mons, Belgium
[3] Physics Laboratory, University of Athens, Solonos Str. 104, GR-10680 Athens, Greece
[4] Department of Physics, University of Bergen, Allégaten 55, N-5007 Bergen, Norway
[5] Dipartimento di Fisica, Università di Bologna and INFN, Via Irnerio 46, I-40126 Bologna, Italy
[6] Collège de France, Lab. de Physique Corpusculaire, 11 pl. M. Berthelot, F-75231 Paris Cedex 05, France
[7] CERN, CH-1211 Geneva 23, Switzerland
[8] Division des Hautes Energies, CRN - Groupe DELPHI and LEPSI, B.P.20 CRO, F-67037 Strasbourg Cedex, France
[9] Institute of Nuclear Physics, N.C.S.R. Demokritos, P.O. Box 60228, GR-15310 Athens, Greece
[10] Dipartimento di Fisica, Università di Genova and INFN, Via Dodecaneso 33, I-16146 Genova, Italy
[11] Institut des Sciences Nucléaires, Université de Grenoble 1, F-38026 Grenoble, France
[12] Research Institute for High Energy Physics, University of Helsinki, Siltavuorenpenger 20 C, SF-00170 Helsinki 17, Finland
[13] Joint Institute for Nuclear Research, Dubna, Head Post Office, P.O. Box 79, 101 000 Moscow, USSR.
[14] Institut für Experimentelle Kernphysik, Universität Karlsruhe, Postfach 6980, D-7500 Karlsruhe 1, FRG
[15] High Energy Physics Laboratory, Institute of Nuclear Physics, Ul. Kawiory 26 a, PL-30055 Krakow 30, Poland
[16] Université de Paris-Sud, Lab. de l'Accélérateur Linéaire, Bat 200, F-91405 Orsay, France
[17] School of Physics and Materials, University of Lancaster - Lancaster LA1 4YB, UK
[18] LIP, Av. Elias Garcia 14 - 1e, P-1000 Lisbon Codex, Portugal
[19] Department of Physics, University of Liverpool, P.O. Box 147, GB - Liverpool L69 3BX, UK
[20] LPNHE, Universités Paris VI et VII, Tour 33 (RdC), 4 place Jussieu, F-75230 Paris Cedex 05, France
[21] Department of Physics, University of Lund, Sölvegatan 14, S-22363 Lund, Sweden
[22] Université Claude Bernard de Lyon, 43 Bd du 11 Novembre 1918, F-69622 Villeurbanne Cedex, France
[23] Universidad Complutense, Avda. Complutense s/n, E-28040 Madrid, Spain
[24] Univ. d'Aix - Marseille II - Case 907 - 70, route Léon Lachamp, F-13288 Marseille Cedex 09, France
[25] Dipartimento di Fisica, Università di Milano and INFN, Via Celoria 16, I-20133 Milan, Italy
[26] Niels Bohr Institute, Blegdamsvej 17, DK-2100 Copenhagen 0, Denmark
[27] NIKHEF-H, Postbus 41882, NL-1009 DB Amsterdam, The Netherlands
[28] National Technical University, Physics Department, Zografou Campus, GR-15773 Athens, Greece
[29] Physics Department, University of Oslo, Blindern, N-1000 Oslo 3, Norway
[30] Nuclear Physics Laboratory, University of Oxford, Keble Road, GB - Oxford OX1 3RH, UK
[31] Dipartimento di Fisica, Università di Padova and INFN, Via Marzolo 8, I-35131 Padua, Italy
[32] Rutherford Appleton Laboratory, Chilton, GB - Didcot OX11 0QX, UK
[33] Dipartimento di Fisica, Università di Roma II and INFN, Tor Vergata, I-00173 Rome, Italy
[34] CEN-Saclay, DPhPE, F-91191 Gif-sur-Yvette Cedex, France
[35] Istituto Superiore di Sanità, Ist. Naz. di Fisica Nucl. (INFN), Viale Regina Elena 299, I-00161 Rome, Italy
[36] Facultad de Ciencias, Universidad de Santander, av. de los Castros, E - 39005 Santander, Spain
[37] Inst. for High Energy Physics, Serpukow P.O. Box 35, Protvino, (Moscow Region), USSR.
[38] Institute of Physics, University of Stockholm, Vanadisvägen 9, S-113 46 Stockholm, Sweden
[39] Dipartimento di Fisica Sperimentale, Università di Torino and INFN, Via P. Giuria 1, I-10125 Turin, Italy
[40] Dipartimento di Fisica, Università di Trieste and INFN, Via A. Valerio 2, I-34127 Trieste, Italy
   and Istituto di Fisica, Università di Udine, I-33100 Udine, Italy
[41] Department of Radiation Sciences, University of Uppsala, P.O. Box 535, S-751 21 Uppsala, Sweden
[42] Inst. de Fisica Corpuscular IFIC, Centro Mixto Univ. de Valencia-CSIC, and Departamento de Fisica Atomica Molecular y Nuclear, Univ. de Valencia, Avda. Dr. Moliner 50, E-46100 Burjassot (Valencia), Spain
[43] Institut für Hochenergiephysik, Österr. Akad. d. Wissensch., Nikolsdorfergasse 18, A-1050 Vienna, Austria
[44] Inst. Nuclear Studies and, University of Warsaw, Ul. Hoza 69, PL-00681 Warsaw, Poland
[45] Fachbereich Physik, University of Wuppertal, Postfach 100 127, D-5600 Wuppertal 1, FRG

1 Introduction

Precise tests of perturbative quantum chromodynamics are made possible by analyzing the large samples of hadronic Z decays collected at LEP. Measurements of the strong coupling constant $\alpha_s(M_Z)$ have been published by the four LEP collaborations ALEPH [1], DELPHI [2], L3 [3]and OPAL [4]. In most of these papers the α_s determination was based either on the measurement of multijet production rates or on the measurement of energy-energy correlations and their asymmetries.

The present paper contains a coherent analysis of the distributions of eight different hadronic observables. Correlations among the α_s values obtained from the different observables are taken into account to derive consistent values of the coupling constant α_s from an original sample of 120600 hadronic events collected in 1990 with the DELPHI detector.

The analysis relies on the numerical calculations of the expansion coefficients of the observables up to order α_s^2 as performed, for instance, by Kunszt and Nason [5]. The fact that the expansion coefficients are limited to second order introduces the well known unphysical dependence of the resulting value of the coupling α_s on the renormalization scale. An averaging procedure was introduced to obtain the central value of $\alpha_s(M_z)$ and its "scale error". For each scale μ the eight values of the coupling constant were averaged by taking into account the correlations between the α_s values from the different observables, and then the average over μ was performed.

Particular attention was paid to the estimate of both the experimental error and the error due to the non-perturbative corrections applied to derive "parton" distributions from the measured hadron distributions. To this end, these hadronization corrections were made using two different approaches: parton shower models and matrix element models. The consistency of the results on $\alpha_s(M_z)$, which are eventually averaged, is an important new outcome of the present analysis.

In Section 2 the relevant parts of the DELPHI detector are briefly described. Section 3 presents the criteria for event selection and analysis. In Section 4 the eight measured hadronic distributions are compared with the expectations of five different fragmentation models. The two methods used to apply hadronic corrections and to derive parton distributions are presented in Section 5. The results and their errors are presented and combined in Section 6. Independent but less precise measurements of $\alpha_s(M_Z)$ obtained from the hadronic and leptonic width of the Z-boson are discussed in Section 7. The final results are summarized in the last Section.

2 The DELPHI Detector

A detailed description of the DELPHI detector can be found in reference [6]. The components relevant for this analysis, namely the tracking system and the electromagnetic calorimeters, will be briefly discussed.

The main tracking system is a 2.7m long time projection chamber (TPC) from 30cm to 122cm in radius. Tracks of charged particles are measured in the TPC with a resolution of $\sim 250\mu m$ in the $r\phi$ projection and $0.9mm$ along the beam direction. The Inner Detector (ID) is a cylindrical wire jet chamber starting at a radius $r = 12cm$ surrounded by a 5 layer proportional chamber. The proportional chamber measures the $r\phi$- and z-coordinates and serves mainly as a fast trigger.

In the barrel region ($43° < \theta < 137°$) the tracking system is completed by the cylindrical

Outer Detector (OD) at $r = 200cm$. It consists of 24 independent modules each containing 5 layers of drift tubes. All planes measure the $r\phi$ coordinate with a resolution of $\sim 110\mu m$. Three layers also provide an approximate z measurement for triggering purposes.

In the forward and backward regions ($11^o < \theta < 33^o$, $147^o < \theta < 169^o$) the tracking is improved by two additional drift chambers. One of them (FCA) is mounted directly on the two TPC endplates. It consists of 3 pairs of wire planes rotated by 120° with respect to each other in order to resolve ambiguities internally. The second set of forward chambers (FCB) is positioned on either side directly in front of the electromagnetic calorimeters. Each consists of 12 planes twice repeating the wire orientations of FCA.

Electromagnetic energy is measured in the barrel part by a high density projection chamber (HPC). It consists of 144 modules arranged in 6 rings around the beam axis. Its fine granularity in all dimensions allows a good two shower separation and electromagnetic particle identification from the shower shape. In the forward region electromagnetic calorimetry is provided by two arrays of 4522 lead glass blocks each, covering the polar angles from 10° to 36.5^o and 143.5^o to 170° respectively.

3   Event Selection and Data Analysis

For this analysis charged particles were used if they fulfilled the following selection criteria:

- momentum between 0.2 GeV/c and 50 GeV/c,
- measured track length larger than 50 cm,
- impact parameter with respect to the fitted main vertex less than 5 cm in the $r\phi$ projection and less than 10 cm along the beam,
- $25^o <$ polar angle (θ) $< 155^o$.

Clusters in the electromagnetic calorimeters were retained if they did not match spatially with a charged particle and if the measured energy was larger than 0.4 GeV. Showers measured by the HPC were also required to be consistent with being induced by a photon.

Events were selected as hadronic events by requiring more than 4 tracks of charged particles and a total energy of all selected charged particles in excess of 12% of the centre of mass energy in total and 3% in each hemisphere. To ensure that the event was well contained in the detector it was additionally required that the angle between the sphericity and the beam axis exceeded 40°. A total of 78905 events survived these cuts. The background from $\tau^+\tau^-$ events was estimated to be about 0.25%; all other backgrounds were below the 0.1% level.

In order to correct the measured distributions for detector effects such as track losses, smearing and secondary interactions and initial state photon radiation, events were generated with the JETSET 7.2 parton shower program [7]combined with the DYMU3 event generator [8]to simulate initial state photon radiation. The generated particles were followed through the detector by a detailed simulation taking into account effects of secondary interactions in the detector material. The simulated data were processed in the same way as the real data. For a quantity X the correction factor C_X was calculated bin by bin as:

$$C_X = \frac{\left(\frac{d\sigma}{dX}\right)_{generated}^{DELSIM}}{\left(\frac{d\sigma}{dX}\right)_{reconstructed}^{DELSIM}} \times \frac{\left(\frac{d\sigma}{dX}\right)^{no\ QED}}{\left(\frac{d\sigma}{dX}\right)^{QED}} \tag{1}$$

DELSIM is the DELPHI full detector simulation program which includes photons from initial state bremsstrahlung (QED radiation). "Generated" means including particles with a lifetime larger than 10^{-9}s without detector simulation whereas on the "reconstructed" level full detector simulation is included. The correction was split into two factors because for the first part, where a full detector simulation is needed, the same events could be used for evaluating the numerator and the denominator which substantially reduces the statistical uncertainties. The second factor could be calculated with much higher statistics without the need of a full detector simulation. The overall correction was typically well within 20% of unity in the regions used for the QCD fits.

To evaluate the systematic errors the cuts for selecting tracks, electromagnetic clusters and events were varied over a wide range. In addition an analysis using only charged particles was performed with events selected to be fully contained in the barrel part of DELPHI. Disagreements between data and Monte Carlo such as additional track losses at the 2% level were simulated and correction factors obtained using different Monte Carlo generators were compared. The systematic errors are quoted in the tables together with the measured distributions.

4 The Event Shape and Comparison with Fragmentation Models

In this Section experimental distributions for eight 3-jet like quantities (i.e. quantities proportional to α_s in lowest order perturbation theory) are presented, namely for thrust T, oblateness O, C-parameter, normalized heavy jet mass squared M_h^2/E_{vis}^2, difference of heavy and light jet mass squared M_d^2/E_{vis}^2, energy-energy correlation EEC and its asymmetry $AEEC$ as well as the differential 2-jet rate D_2. These distributions were selected because predictions in $O(\alpha_s^2)$ perturbation theory for all of these quantities have been worked out in ref. [5]. The experimental results are compared to the corresponding distributions from the Lund JETSET 7.2 parton shower (PS) and matrix element (ME) models [7], the Lund ARIADNE 3.1 colour dipole model [9,10], the NLLJET 2.0 parton shower model [11]of K.Kato and T.Munehisa and the HERWIG 5.1 parton shower model [12]of G.Marchesini and B.R.Webber.

The definitions of event shape variables used in this analysis are as follows:

$$T = \max_{\vec{n}_{thr}} \frac{\sum_i |\vec{p}_i \cdot \vec{n}_{thr}|}{\sum_i |\vec{p}_i|} \tag{2}$$

The thrust axis $\vec{n}_{thr}$ of an event is chosen to maximize the longitudinal momenta along this axis. The normalized sum of these momentum projections (2) is called thrust T[13]. Similarly an axis $\vec{n}_{maj}$ orthogonal to $\vec{n}_{thr}$ can be chosen to maximize the momenta transverse $\vec{n}_{thr}$. The normal vector $\vec{n}_{min}$ is defined by $\vec{n}_{min} = \vec{n}_{thr} \times \vec{n}_{maj}$. The variables major F_{major} and minor F_{minor} are obtained by replacing $\vec{n}_{thr}$ in (2) by $\vec{n}_{maj}$ or $\vec{n}_{min}$, respectively. The Oblateness O[14]then is:

$$O = F_{major} - F_{minor} \tag{3}$$

The so called C-parameter is derived from the eigenvalues λ of the infrared safe momentum tensor Θ^{ij} and does not require the determination of a jet axis [15]:

$$\Theta^{ij} = \frac{1}{\sum_k^{N_{particles}} |\vec{p}_k|} \cdot \sum_k^{N_{particles}} \frac{p_k^i \cdot p_k^j}{|\vec{p}_k|} \quad ; \quad C = 3 \cdot (\lambda_1\lambda_2 + \lambda_2\lambda_3 + \lambda_3\lambda_1) \tag{4}$$

Here p^i denotes the i-th component of the three momentum of the particle in the CMS.

The heavy (light) jet mass M_h (M_l) is defined as the larger (smaller) of the invariant mass of all final state particles in the two event hemispheres separated by the plane normal to the thrust axis. The invariant mass squared is normalized to the visible energy squared E_{vis}^2, i.e. for M_h:

$$\frac{M_h^2}{E_{vis}^2} = \frac{1}{E_{vis}^2} \cdot \max\left(\left(\sum_{\vec{p}_k \cdot \vec{n}_{thr} > 0} p_k\right)^2, \left(\sum_{\vec{p}_k \cdot \vec{n}_{thr} < 0} p_k\right)^2\right) \quad (5)$$

Here p_k denotes the 4-vector of particle k. This definition differs from the original one of Clavelli [16], but has the advantage of being easier to calculate and has therefore also been used by most previous experiments [17]. The difference of the heavy and the light mass M_d^2/E_{vis}^2 was also considered:

$$\frac{M_d^2}{E_{vis}^2} = \frac{M_h^2 - M_l^2}{E_{vis}^2} \quad (6)$$

Here biases due to the fragmentation (contributing both to M_h^2/E_{vis}^2 and M_l^2/E_{vis}^2) are expected to partially cancel.

The energy-energy correlation introduced by Basham et al. [18] is defined from the histogram of angles χ between all particles in an event weighted by their scaled energies:

$$EEC(\chi) = \frac{1}{N}\frac{1}{\Delta\chi}\sum_{events}^{N}\sum_{i,j}^{N_{particles}}\frac{E_iE_j}{E_{vis}^2}\int_{\chi-\frac{\Delta\chi}{2}}^{\chi+\frac{\Delta\chi}{2}}\delta(\chi - \chi_{ij})d\chi \quad (7)$$

where χ_{ij} is the angle between the particles i and j, $\Delta\chi$ is the histogram bin width. Contributions close to 0° arise from particles inside one jet while contributions close to 180° arise from particles in opposite jets. Events with hard gluon radiation contribute asymmetrically to the central χ region. The contribution of 2-jet events cancels out in the energy-energy correlation asymmetry $AEEC$:

$$AEEC(\chi) = EEC(180° - \chi) - EEC(\chi) \quad ; \quad 0° \leq \chi \leq 90° \quad (8)$$

In the present analysis jets were reconstructed in hadronic events by using the y-cluster jet finding algorithm originally introduced by the JADE Collaboration [19]. For each event the squares of the scaled invariant masses y_{ij} for each pair of particles i and j were evaluated:

$$y_{ij} = \frac{2E_iE_j(1 - \cos\theta_{ij})}{E_{vis}^2} \quad , \quad (9)$$

where E_i, E_j are the energies and θ_{ij} the angle between the momentum vectors of the two particles. The particle pair with the lowest value y_{ij} was selected and replaced by a pseudo-particle with four momentum $(p_i + p_j)$, thereby reducing the multiplicity by one. In successive steps the procedure was repeated until the scaled invariant masses of all pairs of pseudo-particles or particles are larger than a given resolution y_{cut}. The remaining pseudo-particles or particles are called jets. This experimental algorithm for reconstructing jet rates corresponds to the theoretical predictions of the E0 - scheme [5].

The differential 2-jet rate D_2 derived from the 2-jet rate R_2 is defined as [20]:

$$D_2(y_{cut}) = \frac{R_2(y_{cut} + \Delta y_{cut}) - R_2(y_{cut})}{\Delta y_{cut}}. \quad (10)$$

QCD Monte Carlo models, which describe well the distributions of the event shape variables in the hadronic final state of e^+e^--annihilation, can be used to estimate how far these distributions are influenced by hadronization effects. The models used in this analysis to estimate the size of these effects and its uncertainty can be classified according to the way they treat the perturbative generation of coloured quarks and gluons and the non-perturbative fragmentation of these partons into colourless hadrons.

The JETSET 7.2 ME model uses the exact $O(\alpha_s^2)$ matrix elements (ME)[21]with an optimized (small) value of the renormalization scale to generate the initial parton configuration with at most four partons.

The HERWIG 5.1 and the JETSET 7.2 PS models use the parton shower (PS) approach [12]derived from the QCD leading logarithmic approximation (LLA) to generate an arbitrary number of primary partons. Angular correlations due to coherence and spin effects are taken into account. The substructure of jets is well described, however the PS approach does not reproduce correctly the number of well separated jets (especially three-jet events). In the JETSET 7.2 PS this deficiency is corrected using a special rejection technique to reproduce the lowest order three-jet cross section [22].

In the ARIADNE 3.1 model the evolution of the parton shower is formulated in terms of colour dipoles. The first dipole is formed by the primary quark and anti-quark. After the emission of a gluon from this colour dipole the subsequent emissions of gluons are given by two independent dipoles built by the quark and the gluon and the gluon and the anti-quark. This strategy is generalized in ARIADNE 3.1 and automatically accounts for angular ordering of the partons as predicted by QCD due to the interference of gluons in the infrared region. ARIADNE 3.1 also produces correct 3-jet rates.

Quantitative tests of QCD cannot easily be performed using PS models because the QCD LLA contains ambiguities. In particular the renormalization scheme is ambiguous and the scale parameter Λ has no well defined meaning. The NLLJET 2.0 model improves this situation, because here the PS evolution is based on the next to leading logarithmic approximation (NLLA). In this approximation (including one loop corrections to the LLA and three body parton splittings) the theoretical ambiguities mentioned above are no longer present.

For the actual fragmentation, i.e. the formation of colourless hadrons, two approaches are used in the above models:

HERWIG 5.1 uses the concept of cluster fragmentation. At the end of the shower development gluons are split into $q\bar{q}$-pairs. The quarks are then combined into clusters obeying colour conservation. These clusters finally decay according to phase space into hadrons.

The other models use the Lund string fragmentation [23]as realized in JETSET 7.2. A colour flux tube or colour string is stretched between the final state partons. Emitted gluons act as kinks or excitations of the string. The string may break and produce a new $q\bar{q}$-pair. This process stops when only on-mass-shell hadrons remain.

A comprehensive overview of these models is given in reference [22]. The JETSET 7.2 program both with matrix element and with parton shower option is run with parameters tuned to DELPHI data [24]. For the Monte Carlo programs ARIADNE 3.1 and HERWIG 5.1 the parameters as determined by OPAL [25]are used. The NLLJET 2.0 program contains the same fragmentation parameters as the JETSET parton shower tuning.

Figs. (1a) to (1h) present the normalized differential cross sections for the different event shape variables together with the predictions of the different Monte Carlo models. The data, including statistical and systematic errors, are also given in Tabs. (1a) to (1g). The curves below the data show the size of the experimental correction factor applied to

the data. The correction factor is about 1.1 to 1.2 for all variables, except for regions near the phase space boundaries. For M_d^2/E_{vis}^2 and O the correction factor is very close to unity over most of the range. All distributions have been obtained from the analysis of charged and neutral particles except those of EEC and $AEEC$. In the case of these two variables the inclusion of neutral particles leads to much bigger acceptance corrections, mainly due to the incomplete coverage with electromagnetic calorimetry in DELPHI, and thus to larger systematic errors.

The JETSET 7.2 PS model and the ARIADNE 3.1 colour dipole model agree best with the data. Only in the $AEEC$ distribution at $65° < \chi < 75°$ the predictions of both models are slightly above the data. However this is also observed for the JETSET 7.2 ME and the NLLJET 2.0 PS model.

The JETSET 7.2 ME model is slightly below the data except for low T, high C, high M_h^2/E_{vis}^2 and high M_d^2/E_{vis}^2 where it is significantly lower. In these regions events with many jets give large contributions. These are expected not to be well represented by the ME model.

The new NLLJET 2.0 model describes the gross shape of all distributions. However, it has a tendency to be above the data for most of the data points. This is presumably due to a too large value of Λ used in the model leading to too many multijet events and too few 2-jet events. At large T and small C where the latter contribute, NLLJET 2.0 is found to be below the data.

Results from HERWIG 5.1 often lie below the data, especially in regions where 3-jet contributions are important, that is at central values of C, T, M_h^2/E_{vis}^2, M_d^2/E_{vis}^2, EEC and especially at large y_{cut} in D_2. Contrary to all other models, HERWIG is below the data in the $AEEC$ distributions at large χ.

5 Comparison with Second Order QCD

All event shape variables discussed in Section 4 (thrust, oblateness, C-parameter, heavy jet mass, jet mass difference, energy-energy correlation, its asymmetry and the jet rates) share the property of being insensitive to the infrared and collinear divergences in perturbative QCD (i.e. they are infrared and collinear safe) and have been calculated to $O(\alpha_s^2)$ at the parton level. For instance, for a shape variable X the weighted differential distribution is given by:

$$\frac{1}{\sigma_{tot}} X \frac{d\sigma}{dX} = \frac{\alpha_s(\mu)}{2\pi} A(X) \left(1 - \frac{\alpha_s(M_Z)}{\pi}\right) + \left(\frac{\alpha_s(\mu)}{2\pi}\right)^2 \cdot \left(A(X) 2\pi b_0 \ln \frac{\mu^2}{s} + B(X)\right) \quad (11)$$

with

$$b_0 = \frac{33 - 2n_f}{12\pi}$$

Here the number of active flavours is denoted by n_f ($= 5$). The functions A and B can be computed by integrating the second order QCD matrix elements calculated by Ellis, Ross and Terrano (ERT) [21]. Their numerical values are specific for each event shape variable. They furthermore depend on additional jet resolution criteria if such are imposed in the $O(\alpha_s^2)$ QCD analysis [26]. This will be discussed later in more detail. For the case where no additional jet resolution criteria are imposed the functions A and B have been computed by Kunszt and Nason [5] for all shape variables used in this analysis.

The running coupling constant α_s at the renormalization scale μ is expressed as

$$\alpha_s(\mu) = \frac{1}{b_0 \ln \frac{\mu^2}{\Lambda^2}} \left(1 - \frac{b_1}{b_0^2} \frac{\ln \ln \frac{\mu^2}{\Lambda^2}}{\ln \frac{\mu^2}{\Lambda^2}} \right) \tag{12}$$

where $\Lambda \equiv \Lambda_{\overline{MS}}^{(5)}$ is the QCD scale parameter, computed in the Modified Minimal Subtraction ($\overline{MS}$) scheme for $n_f = 5$ and $b_1 = (153 - 19n_f)/24\pi^2$.

Perturbation theory in second order leaves the renormalization scale μ undetermined. Recently choices of μ in the range between M_Z and the b-quark mass have been proposed [27]. In the following the quantity $f = \mu^2/M_Z^2$ is conservatively varied in the full range between 0.002 and 1 to estimate the uncertainty due to the unknown higher order corrections.

In equation (11) the differential distribution is normalized to the total hadronic cross section σ_{tot} and not to the leading order cross section σ_0 as in ref. [5]. This results in the correction factor $1 - \alpha_s(M_Z)/\pi$ where the QCD radiative correction to σ_{tot} is evaluated at the renormalization scale M_Z.

In order to compare the measured hadron distributions with the theoretical prediction, hadronization corrections were performed in two different ways:
1. using the parton shower (PS) option of JETSET 7.2,
2. using the ERT matrix element (ME) option of JETSET 7.2.
Both generators use the Lund string fragmentation.

For Method 1, hadronization effects were evaluated according to the method proposed by Magnoli, Nason and Rattazzi [28]by switching on and off the hadronization stage after the full parton shower development. The resulting "experimental bare parton distributions", obtained after applying bin-by-bin corrections to the measured hadron distributions, i.e. multiplying the data by the following ratio of weighted cross sections

$$C_{had} = \left(\frac{1}{\sigma_{tot}} X \frac{d\sigma}{dX} \right)_{parton} \Big/ \left(\frac{1}{\sigma_{tot}} X \frac{d\sigma}{dX} \right)_{hadron} \tag{13}$$

are shown in Figs. (2a) to (2h). The errors presented in these figures contain all randomly distributed errors added in quadrature. Also shown is the size of the hadronization correction as evaluated with the JETSET 7.2 PS program.

$\Lambda_{\overline{MS}}^{(5)}$ and $\alpha_s(M_Z)$ were evaluated by performing fits of the $O(\alpha_s^2)$ expressions (11) to the corresponding bare parton distributions. In these fits the functions A and B tabulated in reference[5]were used and various renormalization scales $\mu^2 = f M_Z^2$ were chosen with f ranging from 0.002 to 1. All fits were performed for a range of values of the shape variables in which

- the contribution from 3 jet events is important
- the experimental detector corrections are small
- the hadronization corrections are small except for oblateness where they amount to about 34%.

Tab. (2) contains the selected fit intervals for the eight distributions.

The functions A and B from ref. [5]do not include mass effects. In order to estimate the effect of quark masses, the evaluation of $\alpha_s(M_Z)$ was repeated but this time by calculating the quantity in the numerator of the correction factor of equation (13) for u-, d- and s-quarks only. This leads to an increase of $\alpha_s(M_Z)$ of 0.002 for the analysis of the distributions in thrust, EEC and C - parameter compared to the result presented in the following section. In all other cases the change of α_s is found to be ±0.001 or even less.

In Method 2, hadronization corrections were evaluated from a retuned version of the ERT matrix element option of JETSET which is known to describe well most of the measured hadronic distributions. In this analysis the default matrix element was used based on the calculation of ERT with the p resolution criterion [5]applied in the derivation of the 3-jet matrix element for all distributions except for the differential jet rates. Due to the introduction of this jet resolution definition $y_{min} > 0$ in the calculation of the dressed $O(\alpha_s^2)$ matrix element, the hadronization correction computed by using the event generator yields corrected data at a dressed level. In addition the event generator takes account of the kinematical effects due to the masses of the generated dressed partons.

While for Method 1 the functions A, B of equation (11) are computed in reference [5]at the bare massless parton level, they have to be recomputed for the α_s analysis of differential distributions corrected to the dressed parton level. The computation can be performed either by using the same ME Monte Carlo generator as used for the hadronization correction or analytically as, for instance, was done for thrust by Gutbrod et al. [26]. In the present work the A, B coefficients were computed from 12 sets of $2 \cdot 10^6$ events simulated with the ERT-p ME generator embedded in JETSET 7.2 for $y_{min} = 0.01$ and a grid of $\Lambda_{\overline{MS}}$ ($50 MeV \leq \Lambda_{\overline{MS}} \leq 400 MeV$) and f ($0.002 \leq f \leq 1$) values. The resulting A, B coefficients were constant within statistical errors except for small values of f and large $\Lambda_{\overline{MS}}$ [†]. Here the three-jet cross section as determined from the ERT matrix element is negative for an important part of the phase space. Therefore the A, B coefficients calculated at small f and large $\Lambda_{\overline{MS}}$ have been excluded from the final averaging. For the analysis of differential jet rates the A, B functions were evaluated by using the JADE cluster algorithm in the ERT-E0 ME Monte Carlo [29]. In this way hadronization corrections could be kept to a minimum.

Since hadronization corrections in Method 2 are larger than in Method 1, they were performed in the following way:

- For the global shape distributions in thrust, oblateness, C-parameter, jet mass, jet mass difference, and differential jet rates the correction matrices M_{ij} connecting bin j at the parton level with bin i at the hadron level were evaluated as follows:

$$\left(\frac{1}{\sigma_{tot}}X\frac{d\sigma}{dX}\right)_i^{hadron} = \sum_j M_{ij}\left(\frac{1}{\sigma_{tot}}X\frac{d\sigma}{dX}\right)_j^{parton} \tag{14}$$

Inserting the parton cross section equation (11) into the right hand side of equation (14) results in the $O(\alpha_s^2)$ expression to be compared with the data.

- For the EEC and AEEC distributions a single event supplies entries into many bins and the correction matrix cannot be evaluated in a straightforward manner. Therefore bin-by-bin corrections were applied before performing QCD fits as in Method 1.

It should be noted that the two methods to correct for hadronization are some kind of extremes. In Method 1 the hadronization corrections are small, since one corrects to a parton level with many (typically nine) gluons, so the parton shower is expected to have a structure already close to the final state hadrons, while in Method 2 the corrections are larger since one corrects to a parton level with at most four partons, as given by the exact second order matrix element.

Both methods have their advantages and disadvantages: The disadvantage of the second method is that the soft and/or collinear gluons have to be cut away in order to

---

[†]We thank J.W. Gary and the OPAL collaboration for pointing out the sensitivity of $\alpha_s$as determined from the $AEEC$ if the A, B coefficients are evaluated at small f and large $\Lambda_{\overline{MS}}$

eliminate the divergent regions in the matrix element, which would otherwise lead to unphysical negative cross sections in the corresponding parts of phase space in the Monte Carlo. The effect of these missing partons has to be simulated by the fragmentation. In case of Method 1 the cut off on the soft- and collinear gluons is much lower: typically an invariant mass of 1 GeV is required between any pair of partons in the PS models, while in the ME models this cut off has to be as high as 13 GeV at $\sqrt{s} = 90$ GeV. The disadvantage of Method 1 is that no exact calculation corresponding to the parton level of the PS model exists and comparing a second order expression with at most two gluons with a parton level with typically nine gluons is only correct if the effect of the additional soft gluons in the parton shower is negligible. However, a comparison of the two methods gives an estimate of the importance of these higher order corrections. Therefore, the complete analysis was done using both methods.

6 Results from the Analysis of Eight Event Shape Distributions

6.1 Experimental Results

Two series of fits to the measured event shape distributions were performed corresponding to the two methods used for applying the hadronization corrections. Values of $\Lambda_{\overline{MS}}$ were determined for each shape distribution for various values of the renormalization scale μ. Using equation (12) the corresponding $\alpha_s(M_Z)$-values were obtained. The results are presented in Figs. (3a) and (3b), which contain the full information that can be extracted from the different experimental distributions.

Tables (2a) and (2b) list for both methods the fit range and (for three values of $f = \mu^2/s$ of 0.002, 0.05, and 0.25) the values of $\alpha_s(M_Z)$, the statistical error, the error due to the systematic uncertainty of the experiment and of the data selection. For Method 1 the systematic uncertainty due to the hadronization correction is also given. The last column indicates the value of χ^2 per number of degrees of freedom for the fits. Since the EEC histogram contains about 15 million entries the pure statistical error in the fit was enlarged by a factor of two to take account of random systematic errors.

The systematic error due to experiment and data analysis has been obtained by repeating the α_s determination:

- for different cuts on the angle between sphericity axis and beam axis,
- with an even stricter event selection which forced all hadronic particles to be fully contained in the barrel part of the detector,
- by using hadronic distributions obtained from analysing charged particles only,
- with different estimates of the track reconstruction efficiencies for charged tracks,
- with a different evaluation of the detector corrections by using the ME option of the JETSET 7.2 Monte Carlo instead of the PS option.

For Method 1 the systematic uncertainty due to the hadronization correction was estimated by repeating the analysis using different models for evaluating the size of this correction: JETSET 7.2 with different tunings, HERWIG 5.1 and ARIADNE 3.1. The NLLJET 2.0 model, with its present tuning, does not describe the data accurately enough and thus its inclusion in the evaluation of the systematic uncertainty due to the hadronization correction was not justified. The hadronization error of Method 1 is in the range $\Delta\alpha_s = \pm0.001$ to ±0.005, varies from observable to observable and also depends on the

scale f (compare Tab. (2a)). The average hadronization error is $\Delta\alpha_s = \pm 0.002$ (hadr.). Since the only ME model available was the JETSET ME model, the systematic error due to the hadronization correction in Method 2 could not be evaluated in the same way as for Method 1. For this reason a larger error was assumed: $\Delta\alpha_s = \pm 0.003$.

Fig. (3a) shows $\alpha_s(M_Z)$ versus $\ln f$ for the case where hadronization corrections were evaluated using the PS option of JETSET 7.2. Some typical errors are indicated, showing the statistical error and the systematic error due to the experiment added in quadrature. Results of the QCD fits are not shown if $\chi^2/NDF > 10$ or if the second order correction diverges. At large values of the scale factor f one observes a rather large spread of the $\alpha_s(M_Z)$ values obtained from the analysis of the different shape distributions, e.g. $0.112 \le \alpha_s \le 0.145$ for $f = 1$. At smaller values of the scale factor a more consistent picture emerges. This may be related to the fact pointed out in reference [30]for the thrust distribution, that small scales simulate the effect of resummed leading and next-to-leading logarithmic terms not accounted for in the theoretical formula. This is also to be expected for the distributions of the other variables used in the present paper.

The results obtained from fits to shape distributions involving hadronization corrections using the ME model are summarized in Fig. (3b) and Tab. (2b). At large f the spread of the $\alpha_s(M_Z)$ values obtained from the eight shape distributions is again large, $0.113 \le \alpha_s \le 0.138$ for $f = 1$, however the curves show a more coherent behaviour than in Fig. (3a).

6.2   Average α_s as Function of the Scale

As already stressed, *the curves of Figs. (3a) and (3b) represent an exhaustive summary of the available experimental information.* There is no unique procedure to obtain from them an average value of α_s with its error because of the (intrinsically ambiguous) dependence of the α_s values from the individual observables on the renormalization scale f. This subject is much debated.

Whatever method is adopted, the strong correlations of the α_s values of the different observables have to be considered when computing any average. For instance, it would be wrong to deduce for $f = 1$ a large value of $\alpha_s(M_Z)$ from the fact that in Fig. (3a) there are several observables giving an α_s value of the order of $\alpha_s = 0.14$, because the eight observables used are not independent.

The following procedure was then developed to compute the average value of $\alpha_s(M_Z)$ for any given f. Firstly, the correlation coefficients ρ^{ij} needed for the calculation of an average were estimated by simulating 60 samples of events from the JETSET 7.2 PS Monte Carlo program. For each sample of events the eight distributions were evaluated and 8 times 60 QCD fits were performed to determine the values α_s^{il} with $l = 1$ to 60 for $f = 0.25$. From these α_s values the error matrix was computed as $C^{ij} = < (\alpha_s^{il} - \alpha_s^i)(\alpha_s^{jl} - \alpha_s^j) >$ with $\alpha_s^i = \sum_l \alpha_s^{il}/60$ and the correlation coefficients $\rho^{ij} = C^{ij}/\sqrt{C^{ii}C^{jj}}$ were obtained. Tab.(3) contains the correlation coefficients obtained for $f = 0.25$. These matrices can be used to compute the average at all values of f, since the final result for α_s changes by much less than 0.001 when using correlation matrices calculated for $f = 0.02$. The matrix elements depend strongly on the cuts and fit intervals used for the individual variables and thus are specific to the present analysis.

The procedure to be adopted from this point on to derive an average value of $\alpha_s(M_Z)$ and its error is not defined and to some extent is arbitrary. Two kinds of averages are implied: one on the values derived from the distributions of the eight observables, the other on the scale factor f. Since the average on the eight observables is better defined,

it was performed first by assuming that the α_s values from all observables were a priori equivalent so that, for the calculation of the average α_s values, equal (but arbitrary) errors were assigned to each measured α_s value. Then for each value of f the average α_s was calculated considering the correlations between the variables determined in the way described above. The errors of these average values were determined by rescaling the initial errors used such that *the χ^2 per degree of freedom was 1 for each f individually.* In doing this the correlations were taken into account. This procedure gives larger errors for the f-values where the spread of the curves of Fig. (3a) is larger. Note that the uncertainty of the α_s values from the individual observables computed in this way were in the range 0.006 to 0.018 for Method 1 and 0.006 to 0.013 for Method 2. The former value in both cases refers to small scales around $f \approx 0.005$, the latter to $f = 1$. Thus the errors found were much larger than the experimental errors or the hadronization errors of the α_s values of the different observables.

The average α_s values as a function of f determined from the points shown in Fig. (3a) for thrust, C-parameter, heavy jet mass, jet mass difference, energy-energy correlation and its asymmetry and the differential jet rates using a hadronization correction obtained with the PS model are shown in Fig. (4a). By comparing these α_s values with those from the individual observables in Fig. (3a) one can gauge the influence of the correlations between the α_s values from the different observables.

Next the average over μ was performed. For this averaging the logarithmic scale of the figures was chosen, as suggested by the appearance of $\ln \mu^2$ in Eqs. 11 and 12. Taking the *weighted* average of the α_s values for the different scales gives $< \alpha_s(M_Z^2) > = 0.115$ indicated by the dashed horizontal line in Fig. (4a). The unweighted average was 0.002 higher. Omitting one variable at a time from the averaging procedure leads to maximal changes of $\Delta\alpha_s = +0.005$ in case of *AEEC* and $\Delta\alpha_s = -0.001$ for T. Combining this average value with the average experimental and hadronization errors from Tab. (2a), Method 1 gives:

$$\text{Method 1}: \quad < \alpha_s(M_Z) > = 0.115 \pm 0.002(exp.) \pm 0.002(hadr.) \qquad (15)$$

Evaluating average values of $\alpha_s(M_Z)$ from the α_s values of the eight observables as function of f by the same method as described above but this time with hadronization corrections being performed using ME models leads to the result shown in Fig. (4b). The same weighted average is $< \alpha_s(M_z) > = 0.111 \pm 0.005$, indicated by the dashed horizontal line in Fig. (4b). The unweighted average is higher by $\Delta\alpha_s = 0.001$. Omitting one variable at a time from the averaging procedure leads to a maximal change of $\Delta\alpha_s = +0.004$ in case of *AEEC*. The largest negative change is smaller than 0.001. The value

$$\text{Method 2}: \quad < \alpha_s(M_Z) > = 0.111 \pm 0.002(exp.) \pm 0.003(hadr.) \qquad (16)$$

is quoted as the result of the analysis where hadronization corrections are evaluated using the ME model. Here a larger systematic error due to the hadronization correction was assumed as for Method 1.

For completeness, in Fig. (4c) the scale dependence of the simple average α_s from the PS and ME analyses is shown.

6.3 Estimate of the Scale Error

Finally the so called "scale" error has to be added to the results (15) and (16). This is the most difficult one to estimate since it is connected to the fact that calculations have only been performed up to $O(\alpha_s^2)$. In fact, if all higher order corrections were known, the

curves of Figs. (3a) and (3b) would be flat and all the values of $\alpha_s(M_Z)$ derived from the different variables would coincide within the experimental and hadronization errors. Thus the last error to be considered is due to the ignorance of higher order QCD terms, and should be indicated as "higher order" correction error. In all previous analyses, when considering one variable at a time, the qualification "scale error" was used for it because it appeared as an unavoidable dependence of $\alpha_s(M_Z)$ on the unknown scale μ. For simplicity the same name is kept even in the present context of a more elaborate consistent multivariable analysis.

The most natural estimate of the error on the average value of α_s is the *average* over f of the errors shown in Figs. (4a) and (4b): the average error ± 0.006 can therefore be interpreted as the scale error. This range is fully compatible with the variation of the average value of $\alpha_s(M_Z)$ in the f-range 0.002 to 1, a criterion often used in the past to obtain the scale error.

Other estimates of the same error follow from the maximum range of α_s values found by using two different approaches:

- Guided by the criteria of "minimal sensitivity (MS)" [31,32], the minima of the curves which appear at different scales in Fig. (3a) give a value of α_s in the range $0.108 \leq \alpha_s(M_Z) \leq 0.119$ for Method 1 and from Fig. (3b) in the range $0.106 \leq \alpha_s(M_Z) \leq 0.117$ for Method 2. The criterion of "fastest apparent convergence (FAC)" [33] gives very similar ranges from M_h^2/E_{vis}^2, M_d^2/E_{vis}^2 and $AEEC$.
- For each of the event shape distributions (except oblateness in case of Method 1) a scale factor f can be found inside the range $0.002 \leq f \leq 1$ so that the analysis is consistent with a value of $\alpha_s(M_Z)$ between 0.112 and 0.119 for Method 1 and $\alpha_s(M_Z)$ between 0.113 and 0.117 for Method 2. This estimate is based on the observation that each observable has its own "optimized" scale so that the common band defines different f-intervals for the various observables.

The corresponding two ranges of α_s for each method partially overlap. The overall uncertainty range from the above criteria is $0.108 \div 0.119$ for Method 1 and $0.106 \div 0.117$ for Method 2. The average difference is ± 0.006 with respect to the corresponding average value, in agreement with the first estimate.

Another estimate of the scale error can be made by computing the variation of α_s when second order corrections are added to first order ones. The second order correction for the average α_s is -0.33. For a simple exponential series this value implies third order corrections of the order of 0.005.

With respect to the central value of $\alpha_s(M_Z)$, it is worth remarking that the MS or FAC criteria prefer α_s values close to the minima of the curves in Figs. (3a) and (3b). As the scale dependences of the individual observables differ, the average α_s determined above is necessarily biased towards values which are too large.

Finally it can be noted that the two methods used to apply the hadronization corrections provided central values which disagree by 0.004 only. This is an independent justification of the magnitude of the scale error because higher order effects were corrected differently in the two analyses.

In conclusion a scale error $\Delta\alpha_s = \pm 0.006$ can be assigned to both methods so that Eqs. (15) and (16) become

$$\text{Method 1}: \quad \alpha_s(M_Z) = 0.115 \pm 0.002(exp.) \pm 0.002(hadr.) \pm 0.006(scale) \qquad (17)$$

$$\text{Method 2}: \quad \alpha_s(M_Z) = 0.111 \pm 0.002(exp.) \pm 0.003(hadr.) \pm 0.006(scale). \qquad (18)$$

6.4   Discussion of the Results

The average value

$$\alpha_s(M_Z) = 0.113 \pm 0.002(exp.) \pm 0.003(hadr.) \pm 0.006(scale) \tag{19}$$

is quoted as the result of a coherent analysis of the event shape distributions where hadronization corrections were performed using PS and ME models. With reference to Fig. (4) it has to be remarked that the central values of α_s are obtained for a scale $f \approx 0.05$ (i.e. for $\mu = 20\text{GeV}$), which can be considered as a reasonable scale.

The errors quoted in Eqs. (17) and (18) do not contain the possible dependence of the correction factors given in Eqs.(13) and (14) on f. In fact in all cases the correction to the parton level has been calculated with a small value of f, since both in the PS and ME models this factor has to be small in order to obtain a good description of the data ($Q^2 = 0.002 \cdot s$ in ME, $Q^2 \approx p_t^2$ of the gluon in PS). The dependence of the results on this assumption was studied by fitting α_s in the ME Monte Carlo directly to the data for four different values of f (0.002, 0.01, 0.1 and 1, respectively). The resulting f dependence of α_s was similar, even after optimizing the fragmentation parameters for each value of f. The absolute values of α_s obtained with this method were compatible with the results of Method 2.

7   Measurement of α_s from the hadronic and leptonic cross sections

The QCD dependence of the hadronic width of the Z-boson has been calculated to 3rd order in α_s [5,34]:

$$
\begin{aligned}
\Gamma_{had} &= \Gamma_{had}^{(\alpha_s=0)} \left[1 + \left(1 + \frac{4m_b^2}{M_Z^2} \frac{3v_b^2 - \frac{3}{2}a_b^2(1 + 2\ln\frac{m_b^2}{M_Z^2})}{\sum_q(a_q^2 + v_q^2)} \right) \frac{\alpha_s}{\pi} \right.\\
&\quad \left. + \left(1.41 + \frac{a_b^2}{\sum_q(a_q^2 + v_q^2)} \frac{I_2(\frac{M_Z}{2m_t})}{3} \right) \left(\frac{\alpha_s}{\pi} \right)^2 - 13 \left(\frac{\alpha_s}{\pi} \right)^3 \right] \tag{20}\\
I_2(\frac{M_Z}{2m_t}) &= 9.25 - 1.037 \left(\frac{M_Z}{2m_t} \right)^2 - 0.632 \left(\frac{M_Z}{2m_t} \right)^4 - 6\ln\frac{M_Z}{m_t}\\
a_q &= 1\\
v_q &= 1 - 4|q|\sin^2\theta_W
\end{aligned}
$$

The term containing the mass of the b-quark, m_b, is given above in 1st order. Neglecting it changes the measured value of α_s only by 0.003. Taking into account leading log corrections to the b-quark mass dependent part [35]lowers α_s by less than 0.001. The top mass (m_t) dependent correction in 2nd order originates from Z-propagator corrections to the axial coupling of the b. Changing m_t from 130 to 180 GeV changes the measurement of α_s by about 0.002. The 3rd order correction of this type is only partially known. Neglecting the complete 3rd term lowers the measured value of α_s by 0.001.

As the hadronic width is strongly affected by loop corrections depending on the unknown masses of the top quark and the Higgs boson it cannot be used directly to determine the strong coupling constant. Those corrections however largely cancel if the

ratio of the hadronic to the leptonic partial width is used instead. If the standard model of electroweak interactions with three massless neutrino species is assumed additional information can be obtained from the relation:

$$\Gamma_Z^{(meas)} = \Gamma_l^{(meas)} \left(\frac{\Gamma_{had}}{\Gamma_l}(\alpha_s) + 3 + 3 \left(\frac{\Gamma_\nu}{\Gamma_l} \right)^{(SM)} \right) \quad (21)$$

In order to take all correlations correctly into account the hadronic and leptonic cross sections measured by DELPHI [36]were refitted using the program ZFITTER of Bardin et al. [37]with free parameters M_Z, Γ_l, α_s, and Γ_Z in case of the model independent fit. The QCD correction was done outside ZFITTER. The top quark mass was fixed in the interval $m_t = 139 \pm 32(stat) \pm 20(m_H)\,GeV$ [38]. The Higgs mass was varied between 50 and 1000 GeV taking the correlation with the top quark mass into account. The results of the fits are:

$$\alpha_s = 0.110 \pm 0.044(exp.) \pm 0.004(m_t, m_H) \quad from \ \frac{\Gamma_{had}}{\Gamma_l},$$
$$\alpha_s = 0.094 \pm 0.035(exp.) \pm 0.004(m_t, m_H) \quad from \ SM \ fit.$$

Although the errors are large it is interesting to observe the good agreement of the α_s determined from the event shapes and the α_s determined using the hadronic width of the Z since in the latter case the theoretical uncertainties and the scale dependence are small and no fragmentation correction is necessary.

8 Conclusions

Differential distributions of eight hadronic shape variables (thrust, oblateness, C-parameter, heavy jet mass and jet mass difference, energy-energy correlation and its asymmetry and differential jet rates) corrected for initial state photon radiation and detector effects have been measured at $\sqrt{s} = M_Z$ by the DELPHI collaboration. The data were compared to the predictions of various QCD-based models. In order to test quantitatively the consistency of the results calculated with QCD to order α_s^2, an analysis was performed for each of the distributions after evaluating the hadronization effects with two methods. In both cases the renormalization scale μ was allowed to vary between less than m_b and M_Z. When the hadronization corrections were calculated by using parton shower models, the analysis gave $\alpha_s(M_Z) = 0.115 \pm 0.002(exp.) \pm 0.002(hadr.) \pm 0.006(scale)$. Here the first error contains the statistical error and the systematic experimental uncertainty, the second represents the systematic uncertainty of the hadronization corrections using parton shower models, and the third indicates the spread of α_s values due to missing higher order corrections in the theoretical calculations as far as it could be estimated in the framework of the present $O(\alpha_s^2)$ analysis. The corresponding result obtained when hadronization corrections were evaluated by using the matrix element model is $\alpha_s(M_Z) = 0.111 \pm 0.002(exp.) \pm 0.003(hadr.) \pm 0.006(scale)$. In both analyses the correlations between the α_s values from the different observables were taken into account when evaluating the average α_s values.

In conclusion the value

$$\alpha_s(M_Z) = 0.113 \pm 0.007$$

is the final result obtained from the analysis of eight event shape distributions. An additional measurement of α_s from hadronic and leptonic cross sections yielded results in agreement with this value but with much larger errors.

The result is in good agreement with a recent analysis [39]of deep inelastic structure functions [40] which lead to $\alpha_s(M_Z) = 0.109^{+0.007}_{-0.008}$ and with previous LEP results [1-4].

References

[1] ALEPH collab., D. Decamp et al., Phys. Lett. B255 (1991) 623,
    ALEPH collab., D. Decamp et al., Phys. Lett. B257 (1991) 479.

[2] DELPHI collab., P. Abreu et al., Phys. Lett. B247 (1990) 167,
    DELPHI collab., P. Abreu et al., Phys. Lett. B252 (1990) 149.

[3] L3 collab., B. Adeva et al., Phys. Lett. B248 (1990) 464,
    L3 collab., B. Adeva et al., Phys. Lett. B257 (1991) 469.

[4] OPAL collab., M.Z. Akrawy et al., Phys. Lett. B235 (1990) 389,
    OPAL collab., M.Z. Akrawy et al., Phys. Lett. B252 (1990) 159,
    OPAL collab., M.Z. Akrawy et al., Zeit. Phys. C49 (1991) 375.

[5] Z. Kunszt and P. Nason, Z Physics at LEP 1, CERN 89-08, Vol. 1.

[6] DELPHI collab., P. Aarnio et al., Nucl. Inst. Meth. A303 (1991) 233.

[7] T. Sjöstrand, Comp.Phys.Comm. 27 (1982) 243, ibid. 28 (1983) 229,
    T. Sjöstrand and M. Bengtsson, Comp.Phys.Comm. 43 (1987) 367.

[8] J.E. Campagne and R. Zitoun, Zeit. Phys. C43 (1989) 469.

[9] B. Anderson et al., Phys.Rep. 97 (1983) 33,
    T. Gottschalk, D. Morris CALT-68-1365 (1986).

[10] L. Lönnblad, 'A Manual for Ariadne Version 3', LU TP 89-10 (1989),
    L. Lönnblad and U. Petterson, LU TP 88-15 (1988),
    U. Petterson, 'Ariadne, A Monte Carlo for QCD Cascades in the Colour Dipole
    Formulation', LU TP 88-5 (1988).

[11] K. Kato and T. Munehisa, CERN-TH 5719 /90.

[12] G. Marchesini and B.R. Webber, Nucl. Phys. B238 (1984) 1,
    G. Marchesini and B.R. Webber, Nucl. Phys. B310 (1988) 461,
    G. Marchesini and B.R. Webber, Nucl. Phys. B330 (1990) 261,
    G. Marchesini and B.R. Webber, Nucl. Phys. B349 (1991) 635.

[13] S. Brandt, Ch. Peyrou, R. Sosnowski, A. Wroblewski, Phys. Lett. 12 (1964) 57
    E. Farhi, Phys.Rev.Lett. 39 (1977) 1587.

[14] Mark J Coll., D.P. Barber et al., Phys. Rev. Lett. 43 (1979) 830,
    Mark J Coll., D.P. Barber et al., Phys. Lett. B89 (1979) 132,
    Mark J Coll., D.P. Barber et al., Phys. Lett. B108 (1982) 63.

[15] G. Parisi, Phys. Lett. B74 (1978) 65,
    J.F. Donoghue, F. E. Low and S.Y. Pi, Phys. Rev. D20 (1979) 107.

[16] L. Clavelli, Phys. Lett. B85 (1979) 111.

[17] Mark II collaboration, A. Petersen et al., Phys. Rev. D37 (1988) 1,
    TASSO collaboration, W. Braunschweig et al., Z. Phys. C45 (1989) 11.

[18] C.L. Basham, L.S. Brown, S.D. Ellis, T. Love, Phys. Rev. Lett. 41 (1978) 1585.

[19] JADE collab., W. Bartel et al., Zeit. Phys. C33 (1986) 23,
    S.Bethke et al., Phys. Lett. B213 (1988) 235.

[20] L. Smolik, PhD Thesis, University of Heidelberg (1989).

[21] R.K. Ellis, D.A. Ross and E.A. Terrano, Nucl. Phys. B178 (1981) 421.

[22] QCD Generators, B. Bambah et al. in Physics at LEP 1, CERN 89-08, Vol. 3,
    p. 143.

[23] X. Artru, G. Mennessier, Nucl. Phys. B70 (1974) 93,
    B. Anderson et al., Phys. Rep. 97 (1983) 33.

[24] DELPHI Note, Comparison of DELPHI data with QCD models, Contribution
    to LP-HEP 91 Conference, Geneva 1991.

[25] OPAL collab., M.Z. Akrawy et al., Zeit. Phys. C47 (1990) 505.

[26] F. Gutbrod, G. Kramer, G. Rudolph, G. Schierholz, Zeit. Phys. C35 (1987) 543.

[27] W.J. Stirling, University of Durham Preprint DTP/91/04 (1991),
to be published in Journal of Physics G.

[28] N. Magnoli, P. Nason, R. Rattazzi, CERN-TH 5844/90.

[29] N. Magnussen, DESY Report F22-89-01 (1989).

[30] S. Catani, G.Turnock, B.R. Webber and L. Trentadue, Cavendish-HEP 91-3 (1991).

[31] P.M. Stevenson, Nucl. Phys. B203 (1982) 472,
P.M. Stevenson, Nucl. Phys. B231 (1984) 65.

[32] G. Kramer and B. Lampe, Zeit. Phys. C39 (1988) 101.

[33] G. Grunberg, Phys. Lett. B95 (1980) 70.

[34] S.G. Gorishny, A.L. Kataev and S.A. Larin, Phys. Lett. B259 (1991) 144,
L.R. Surguladze, M.A. Samuel, PRL 66 (1991) 560, Erratum ibid 66 (1991) 2416.

[35] K.G. Chetyrkin, J.H. Kühn, Phys. Lett. B248 (1990) 359.

[36] DELPHI collab., P. Abreu et al., Nucl. Phys. B367 (1991) 511.

[37] D. Bardin et al., Zeit. Phys. C44 (1989) 493, Comp. Phys. Comm. 59 (1990) 303,
Nucl. Phys. B 351 (1991) 1.

[38] F. Dydak, Results from LEP and the SLC, Proceedings of the 25th International Conference on High Energy Physics, Singapore 1990, K.X.Phua and Y.Yamaguchi eds. (1991)3.

[39] A.D. Martin, W.J. Stirling and R.G. Roberts, RAL-91-044, DTP/91/24 (1991).

[40] BCDMS collab.: A.C. Benvenuti et al., Phys. Lett. B 223 (1989) 485,
CDHSW collab.: J.P. Berge et al., Zeit. Phys. C 49 (1990) 187,
NMC: D. Allasia et al., Phys. Lett. B 294 (1990) 366,
BCDMS collab.: A.C. Benvenuti et al., Phys. Lett. B 237 (1990) 599,
EMC: J.J. Aubert et al., Nucl. Phys. B 293 (1987) 740,
WA70 collab.: M. Bonesini et al., Zeit. Phys. C 38 (1988) 371.

Table Captions

Table 1: Experimental differential distributions of the thrust T (1a), the oblateness O (1b), the C-parameter C (1c), the heavy mass M_h^2/E_{vis}^2 (1d), the difference of the heavy and light mass M_d^2/E_{vis}^2 (1e), the energy-energy correlation EEC as a function of the correlation angle χ (1f) and the differential 2-jet rate D_2 as a function of y_{cut} (1g). The first error represents the statistical uncertainty and the second error represents the experimental systematic uncertainty.

Table 2: Values of $\alpha_s(M_Z)$ from a fit at three different scales μ^2/M_Z^2 for the distributions thrust T, oblateness O, C-parameter C, heavy mass M_h^2/E_{vis}^2, difference of the heavy and light mass M_d^2/E_{vis}^2, energy-energy correlation EEC and its asymmetry $AEEC$ and the differential 2-jet rate D_2. In Table (2a) the hadronization corrections are obtained with a parton shower Monte Carlo. In Table (2b) the hadronization corrections are done with a matrix element Monte Carlo.

Table 3: Correlation coefficients as used for the PS analysis (above the diagonal) and the ME analysis (below the diagonal). The statistical error of the coefficients is of the order 10%.

Figure Captions

Figure 1: Experimental differential distributions of the thrust T (1a), the oblateness O (1b), the C-parameter C (1c), the heavy mass M_h^2/E_{vis}^2 (1d), the difference of the heavy and light mass M_d^2/E_{vis}^2 (1e), the energy-energy correlation EEC (1f) and its asymmetry $AEEC$ (1g) and the differential 2-jet rate D_2 (1h) in comparison to the predictions of the JETSET 7.2 (PS) and (ME) model, the HERWIG 5.1 model, the NLLJET 2.0 model and the ARIADNE 3.1 model. Comments on the tuning of the hadronic event generators are given in section 4. The errors shown are statistical only. The detector corrections applied to the data are shown in the curves below the data.

Figure 2: Experimental bare parton distributions of the thrust T (2a), the oblateness O (2b), the C-parameter C (2c), the heavy mass M_h^2/E_{vis}^2 (2d), the difference of the heavy and light mass M_d^2/E_{vis}^2 (2e), the energy-energy correlation EEC (2f) and its asymmetry $AEEC$ (2g) and the differential 2-jet rate D_2 (2h). The errors shown contain all randomly distributed errors added in quadrature. The curves are fits to the data as described in the text. The scale parameter is set to $f = 0.25$. The hadronization corrections as calculated with the JETSET 7.2 PS model applied to the data are shown in the curves below the parton distributions.

Figure 3: Values of $\alpha_s(M_Z)$ at different scales of μ^2/M_Z^2 for the distributions thrust T, oblateness O, C-parameter C, heavy mass M_h^2/E_{vis}^2, difference of the heavy and light mass M_d^2/E_{vis}^2, energy-energy correlation EEC and its asymmetry $AEEC$ and the differential 2-jet rate D_2. The errors show some typical statistical and experimental systematic errors added in quadrature. The hadronization corrections are done with the JETSET 7.2 PS

model in (3a). The hadronization corrections are done with the JETSET 7.2 ME model in (3b).

Figure 4: Averaged values of $\alpha_s(M_Z)$ at different scales of μ^2/M_Z^2 for hadronization corrections done with the JETSET 7.2 PS model (4a) and with the JETSET 7.2 ME model (4b). The errorbands shown indicate the disagreement between the α_s values obtained from the different observables due to missing higher order corrections in the theoretical calculations.

T	$1/\sigma_{tot}\ d\sigma/dT$
0.625	$0.025 \pm 0.005 \pm 0.003$
0.675	$0.135 \pm 0.009 \pm 0.008$
0.725	$0.315 \pm 0.015 \pm 0.013$
0.770	$0.529 \pm 0.017 \pm 0.016$
0.810	$0.918 \pm 0.029 \pm 0.018$
0.845	$1.394 \pm 0.041 \pm 0.028$
0.875	$2.091 \pm 0.051 \pm 0.063$
0.900	$3.204 \pm 0.079 \pm 0.130$
0.920	$4.54 \pm 0.09\ \ \pm 0.18$
0.940	$6.84 \pm 0.11\ \ \pm 0.27$
0.955	$10.02 \pm 0.19\ \ \pm 0.40$
0.965	$13.87 \pm 0.22\ \ \pm 0.55$
0.975	$16.46 \pm 0.23\ \ \pm 1.15$
0.985	$10.08 \pm 0.16\ \ \pm 0.71$
0.995	$1.22 \pm 0.05\ \ \pm 0.12$

Table 1a: Thrust distribution

O	$1/\sigma_{tot}\ d\sigma/dO$
0.01	$9.09 \pm 0.13\ \ \pm 0.45$
0.03	$11.17 \pm 0.14\ \ \pm 0.23$
0.05	$7.13 \pm 0.11\ \ \pm 0.14$
0.07	$4.69 \pm 0.09\ \ \pm 0.09$
0.09	$3.603 \pm 0.079\ \ \pm 0.072$
0.12	$2.521 \pm 0.047\ \ \pm 0.050$
0.16	$1.595 \pm 0.037\ \ \pm 0.032$
0.20	$1.042 \pm 0.029\ \ \pm 0.021$
0.25	$0.684 \pm 0.020\ \ \pm 0.014$
0.31	$0.368 \pm 0.014\ \ \pm 0.011$
0.38	$0.1642 \pm 0.0075 \pm 0.0066$
0.46	$0.0395 \pm 0.0033 \pm 0.0019$

Table 1b: Oblateness distribution

C	$1/\sigma_{tot}\ d\sigma/dC$
0.03	$0.36 \pm 0.01\ \ \pm 0.02$
0.07	$2.02 \pm 0.04\ \ \pm 0.04$
0.09	$3.33 \pm 0.06\ \ \pm 0.06$
0.11	$3.76 \pm 0.07\ \ \pm 0.12$
0.13	$3.79 \pm 0.07\ \ \pm 0.12$
0.15	$3.42 \pm 0.07\ \ \pm 0.11$
0.17	$2.98 \pm 0.06\ \ \pm 0.10$
0.20	$2.52 \pm 0.04\ \ \pm 0.10$
0.24	$1.92 \pm 0.04\ \ \pm 0.08$
0.28	$1.60 \pm 0.03\ \ \pm 0.05$
0.32	$1.38 \pm 0.03\ \ \pm 0.03$
0.36	$1.14 \pm 0.03\ \ \pm 0.02$
0.41	$0.94 \pm 0.02\ \ \pm 0.02$
0.47	$0.75 \pm 0.02\ \ \pm 0.02$
0.53	$0.61 \pm 0.02\ \ \pm 0.02$
0.59	$0.52 \pm 0.02\ \ \pm 0.02$
0.66	$0.40 \pm 0.01\ \ \pm 0.02$
0.74	$0.31 \pm 0.01\ \ \pm 0.03$
0.82	$0.17 \pm 0.07\ \ \pm 0.03$
0.93	$0.098 \pm 0.004 \pm 0.04$

Table 1c: C-parameter distribution

M_h^2/E_{vis}^2	$1/\sigma_{tot}\ d\sigma/d(M_h^2/E_{vis}^2)$	
0.005	2.86 ± 0.06	± 0.06
0.015	18.59 ± 0.20	± 0.40
0.025	20.08 ± 0.25	± 0.40
0.035	13.29 ± 0.20	± 0.26
0.045	9.08 ± 0.16	± 0.18
0.055	6.59 ± 0.14	± 0.13
0.065	5.11 ± 0.12	± 0.10
0.075	4.13 ± 0.11	± 0.08
0.090	3.04 ± 0.07	± 0.06
0.110	2.07 ± 0.06	± 0.04
0.130	1.47 ± 0.05	± 0.03
0.150	1.06 ± 0.04	± 0.03
0.170	0.71 ± 0.03	± 0.02
0.190	0.52 ± 0.03	± 0.02
0.215	0.37 ± 0.02	± 0.01
0.245	0.20 ± 0.01	± 0.01
0.275	0.096 ± 0.008	± 0.01
0.305	0.040 ± 0.005	± 0.008
0.340	0.0058 ± 0.001	± 0.0023
0.380	0.0015 ± 0.0007	± 0.0012

Table 1d: Heavy jet mass distribution

M_d^2/E_{vis}^2	$1/\sigma_{tot}\, d\sigma/d(M_d^2/E_{vis}^2)$	
0.005	34.06 ± 0.30	± 0.70
0.015	20.88 ± 0.24	± 0.42
0.025	11.32 ± 0.17	± 0.22
0.035	7.45 ± 0.14	± 0.18
0.045	4.97 ± 0.11	± 0.10
0.055	4.06 ± 0.11	± 0.09
0.065	3.03 ± 0.09	± 0.07
0.075	2.41 ± 0.08	± 0.06
0.090	1.71 ± 0.05	± 0.04
0.110	1.28 ± 0.04	± 0.04
0.130	0.90 ± 0.04	± 0.03
0.150	0.64 ± 0.03	± 0.02
0.170	0.43 ± 0.02	± 0.02
0.190	0.31 ± 0.02	± 0.02
0.215	0.20 ± 0.01	± 0.02
0.245	0.12 ± 0.01	± 0.01
0.275	0.045 ± 0.005	± 0.012
0.305	0.018 ± 0.003	± 0.007
0.340	$0.0021 \pm 0.0005 \pm 0.0013$	
0.380	$0.0006 \pm 0.0003 \pm 0.0005$	

Table 1e: Distribution of difference between square of heavy and light jet mass

$\chi[°]$	$EEC(180° - \chi)$	$EEC(\chi)$
1.8	$0.7286 \pm 0.0069 \pm 0.0272$	$2.1810 \pm 0.0043 \pm 0.0409$
5.4	$1.2404 \pm 0.0079 \pm 0.0284$	$1.2809 \pm 0.0037 \pm 0.0393$
9.0	$1.0666 \pm 0.0055 \pm 0.0165$	$0.8937 \pm 0.0028 \pm 0.0271$
12.6	$0.8250 \pm 0.0022 \pm 0.0095$	$0.6141 \pm 0.0024 \pm 0.0133$
16.2	$0.6312 \pm 0.0020 \pm 0.0103$	$0.4395 \pm 0.0012 \pm 0.0147$
19.8	$0.4873 \pm 0.0023 \pm 0.0096$	$0.3280 \pm 0.0011 \pm 0.0123$
23.4	$0.3891 \pm 0.0020 \pm 0.0067$	$0.2588 \pm 0.0006 \pm 0.0101$
27.0	$0.3183 \pm 0.0030 \pm 0.0068$	$0.2115 \pm 0.0009 \pm 0.0071$
30.6	$0.2682 \pm 0.0019 \pm 0.0053$	$0.1794 \pm 0.0008 \pm 0.0045$
34.2	$0.2249 \pm 0.0009 \pm 0.0036$	$0.1557 \pm 0.0007 \pm 0.0027$
37.8	$0.1972 \pm 0.0014 \pm 0.0032$	$0.1394 \pm 0.0009 \pm 0.0025$
41.4	$0.1729 \pm 0.0013 \pm 0.0026$	$0.1267 \pm 0.0008 \pm 0.0025$
45.0	$0.1543 \pm 0.0012 \pm 0.0024$	$0.1163 \pm 0.0006 \pm 0.0020$
48.6	$0.1411 \pm 0.0011 \pm 0.0025$	$0.1082 \pm 0.0005 \pm 0.0021$
52.2	$0.1273 \pm 0.0009 \pm 0.0021$	$0.1017 \pm 0.0005 \pm 0.0020$
55.8	$0.1173 \pm 0.0011 \pm 0.0020$	$0.0956 \pm 0.0006 \pm 0.0018$
59.4	$0.1102 \pm 0.0012 \pm 0.0020$	$0.0910 \pm 0.0004 \pm 0.0018$
63.0	$0.1030 \pm 0.0011 \pm 0.0018$	$0.0889 \pm 0.0007 \pm 0.0018$
66.6	$0.0971 \pm 0.0008 \pm 0.0018$	$0.0857 \pm 0.0005 \pm 0.0016$
70.2	$0.0921 \pm 0.0009 \pm 0.0017$	$0.0823 \pm 0.0005 \pm 0.0015$
73.8	$0.0877 \pm 0.0008 \pm 0.0017$	$0.0810 \pm 0.0007 \pm 0.0015$
77.4	$0.0857 \pm 0.0010 \pm 0.0017$	$0.0792 \pm 0.0007 \pm 0.0014$
81.0	$0.0824 \pm 0.0008 \pm 0.0016$	$0.0789 \pm 0.0009 \pm 0.0014$
84.6	$0.0817 \pm 0.0007 \pm 0.0016$	$0.0788 \pm 0.0007 \pm 0.0014$
88.2	$0.0808 \pm 0.0012 \pm 0.0015$	$0.0795 \pm 0.0009 \pm 0.0015$

Table 1f: EEC distribution

y_{cut}	$D_2(y_{cut})$
0.00 - 0.01	$24.84 \pm 0.26 \pm 0.60$
0.01 - 0.02	$17.97 \pm 0.24 \pm 0.36$
0.02 - 0.03	$11.87 \pm 0.21 \pm 0.24$
0.03 - 0.04	$8.36 \pm 0.18 \pm 0.18$
0.04 - 0.05	$6.25 \pm 0.15 \pm 0.15$
0.05 - 0.06	$4.97 \pm 0.14 \pm 0.12$
0.06 - 0.08	$3.75 \pm 0.11 \pm 0.09$
0.08 - 0.10	$2.63 \pm 0.08 \pm 0.06$
0.10 - 0.12	$1.72 \pm 0.06 \pm 0.04$
0.12 - 0.14	$1.34 \pm 0.05 \pm 0.03$
0.14 - 0.16	$1.02 \pm 0.04 \pm 0.03$
0.16 - 0.18	$0.74 \pm 0.04 \pm 0.03$
0.18 - 0.20	$0.63 \pm 0.03 \pm 0.04$
0.20 - 0.22	$0.46 \pm 0.03 \pm 0.04$
0.22 - 0.25	$0.31 \pm 0.02 \pm 0.04$
0.25 - 0.28	$0.18 \pm 0.01 \pm 0.03$
0.28 - 0.31	$0.07 \pm 0.01 \pm 0.02$
0.31 - 0.32	$0.03 \pm 0.01 \pm 0.02$

Table 1g: Differential 2-jet rate distribution

Variable Fit Range NDF	Scale f	$\alpha_S(M_Z)$ stat. exp. hadr.	χ^2/NDF
T	0.250	$0.135 \pm 0.001 \pm 0.001 \pm 0.001$	1.2
0.7-0.9	0.050	$0.125 \pm 0.001 \pm 0.001 \pm 0.001$	1.1
19	0.002	$0.112 \pm 0.001 \pm 0.001 \pm 0.001$	1.1
O	0.250	$0.145 \pm 0.003 \pm 0.003 \pm 0.004$	2.3
0.1-0.3	0.050	$0.134 \pm 0.002 \pm 0.001 \pm 0.001$	40.
9	0.002		
C	0.250	$0.133 \pm 0.001 \pm 0.002 \pm 0.001$	1.3
0.32-0.68	0.050	$0.124 \pm 0.001 \pm 0.001 \pm 0.001$	1.3
16	0.002	$0.111 \pm 0.001 \pm 0.001 \pm 0.001$	1.2
M_h^2/E_{vis}^2	0.250	$0.129 \pm 0.002 \pm 0.001 \pm 0.004$	0.6
0.05-0.20	0.050	$0.123 \pm 0.002 \pm 0.001 \pm 0.003$	0.6
14	0.002	$0.121 \pm 0.002 \pm 0.001 \pm 0.003$	0.3
M_d^2/E_{vis}^2	0.250	$0.120 \pm 0.001 \pm 0.002 \pm 0.004$	1.6
0.06-0.20	0.050	$0.119 \pm 0.001 \pm 0.002 \pm 0.004$	1.5
13	0.002	$0.115 \pm 0.001 \pm 0.001 \pm 0.001$	29.
EEC	0.250	$0.123 \pm 0.001 \pm 0.001 \pm 0.001$	2.8
-0.72-0.72	0.050	$0.117 \pm 0.001 \pm 0.001 \pm 0.001$	2.6
35	0.002	$0.111 \pm 0.001 \pm 0.001 \pm 0.001$	7.5
$AEEC$	0.250	$0.110 \pm 0.001 \pm 0.003 \pm 0.005$	1.5
0.12-1.0	0.050	$0.108 \pm 0.001 \pm 0.003 \pm 0.004$	1.9
21	0.002	$0.111 \pm 0.001 \pm 0.001 \pm 0.002$	14.
D_2	0.250	$0.123 \pm 0.001 \pm 0.001 \pm 0.001$	0.7
0.05-0.15	0.050	$0.117 \pm 0.001 \pm 0.001 \pm 0.001$	0.6
9	0.002	$0.112 \pm 0.001 \pm 0.001 \pm 0.001$	0.5

Table 2a: PS fit results and errors

Variable Fit Range NDF	Scale f	$\alpha_S(M_Z)$ stat. exp.	χ^2/NDF
T	0.250	$0.129 \pm 0.001 \pm 0.001$	1.5
0.7-0.9	0.050	$0.121 \pm 0.001 \pm 0.001$	1.4
19	0.002	$0.111 \pm 0.001 \pm 0.001$	1.6
O	0.250	$0.111 \pm 0.002 \pm 0.001$	0.2
0.1-0.3	0.050	$0.107 \pm 0.002 \pm 0.001$	0.2
9	0.002	$0.109 \pm 0.002 \pm 0.001$	0.7
C	0.250	$0.127 \pm 0.001 \pm 0.002$	1.7
0.34-0.70	0.050	$0.120 \pm 0.001 \pm 0.001$	1.4
16	0.002	$0.112 \pm 0.001 \pm 0.001$	1.0
M_h^2/E_{vis}^2	0.250	$0.127 \pm 0.001 \pm 0.001$	1.9
0.08-0.20	0.050	$0.120 \pm 0.001 \pm 0.001$	1.8
10	0.002	$0.115 \pm 0.001 \pm 0.001$	1.5
M_d^2/E_{vis}^2	0.250	$0.122 \pm 0.001 \pm 0.002$	1.7
0.06-0.20	0.050	$0.118 \pm 0.001 \pm 0.002$	1.6
13	0.002	$0.126 \pm 0.001 \pm 0.003$	1.7
EEC	0.250	$0.120 \pm 0.001 \pm 0.001$	1.5
-0.72-0.72	0.050	$0.114 \pm 0.001 \pm 0.001$	0.6
35	0.002	$0.107 \pm 0.001 \pm 0.001$	2.6
$AEEC$	0.250	$0.110 \pm 0.001 \pm 0.002$	1.0
0.12-1.0	0.050	$0.107 \pm 0.001 \pm 0.002$	0.9
21	0.002	$0.114 \pm 0.001 \pm 0.002$	3.5
D_2	0.250	$0.117 \pm 0.001 \pm 0.001$	1.0
0.05-0.15	0.050	$0.111 \pm 0.001 \pm 0.001$	0.7
9	0.002	$0.106 \pm 0.001 \pm 0.001$	0.5

Table 2b: ME fit results and errors

		PS								
		T	C	M_h^2/E_{vis}^2	M_d^2/E_{vis}^2	EEC	$AEEC$	D_2		
	T	1	0.54	0.55	0.59	0.77	0.56	0.32	T	
	C	0.69	1	0.77	0.61	0.66	0.33	0.45	C	
	M_h^2/E_{vis}^2	0.73	0.58	1	0.59	0.68	0.33	0.46	M_h^2/E_{vis}^2	
M	M_d^2/E_{vis}^2	0.55	0.47	0.71	1	0.61	0.34	0.44	M_d^2/E_{vis}^2	P
E	EEC	0.52	0.56	0.51	0.51	1	0.75	0.28	EEC	S
	$AEEC$	0.61	0.44	0.48	0.38	0.68	1	-0.05	$AEEC$	
	D_2	0.34	0.52	0.33	0.48	0.36	0.19	1	D_2	
	O	0.23	0.32	0.21	0.45	0.43	0.11	0.54		
		T	C	M_h^2/E_{vis}^2	M_d^2/E_{vis}^2	EEC	$AEEC$	D_2		
		ME								

Table 3: correlation coefficients for the PS analysis (above diagonal) and the ME analysis (below diagonal)

28

DELPHI

- ● DATA 90
- —— JETSET 7.2 PS
- - - - - JETSET 7.2 ME
- ········ HERWIG 5.1 PS
- ·-·-· NLLJET 2.0 PS
- ·-··-· ARIADNE 3.1 PS
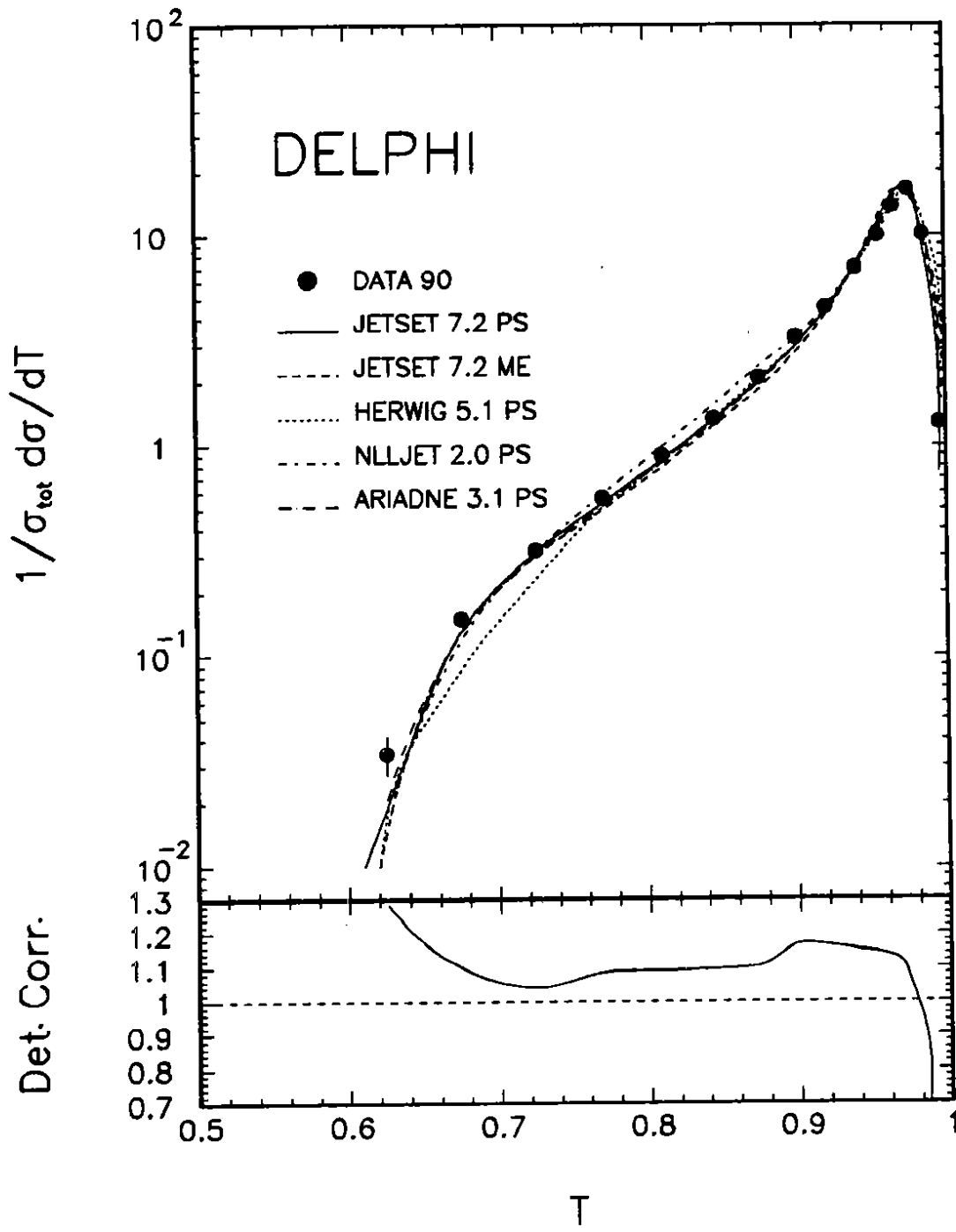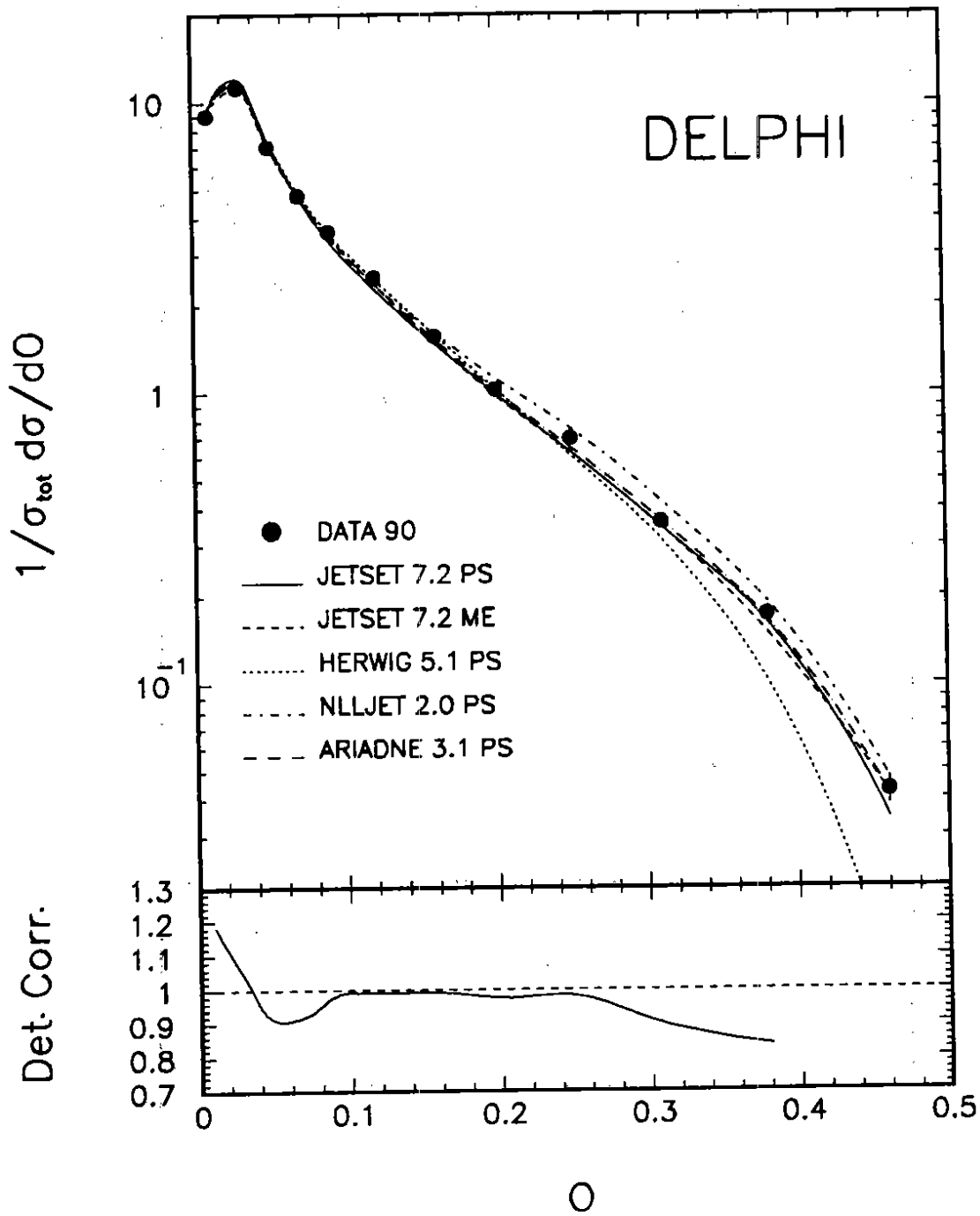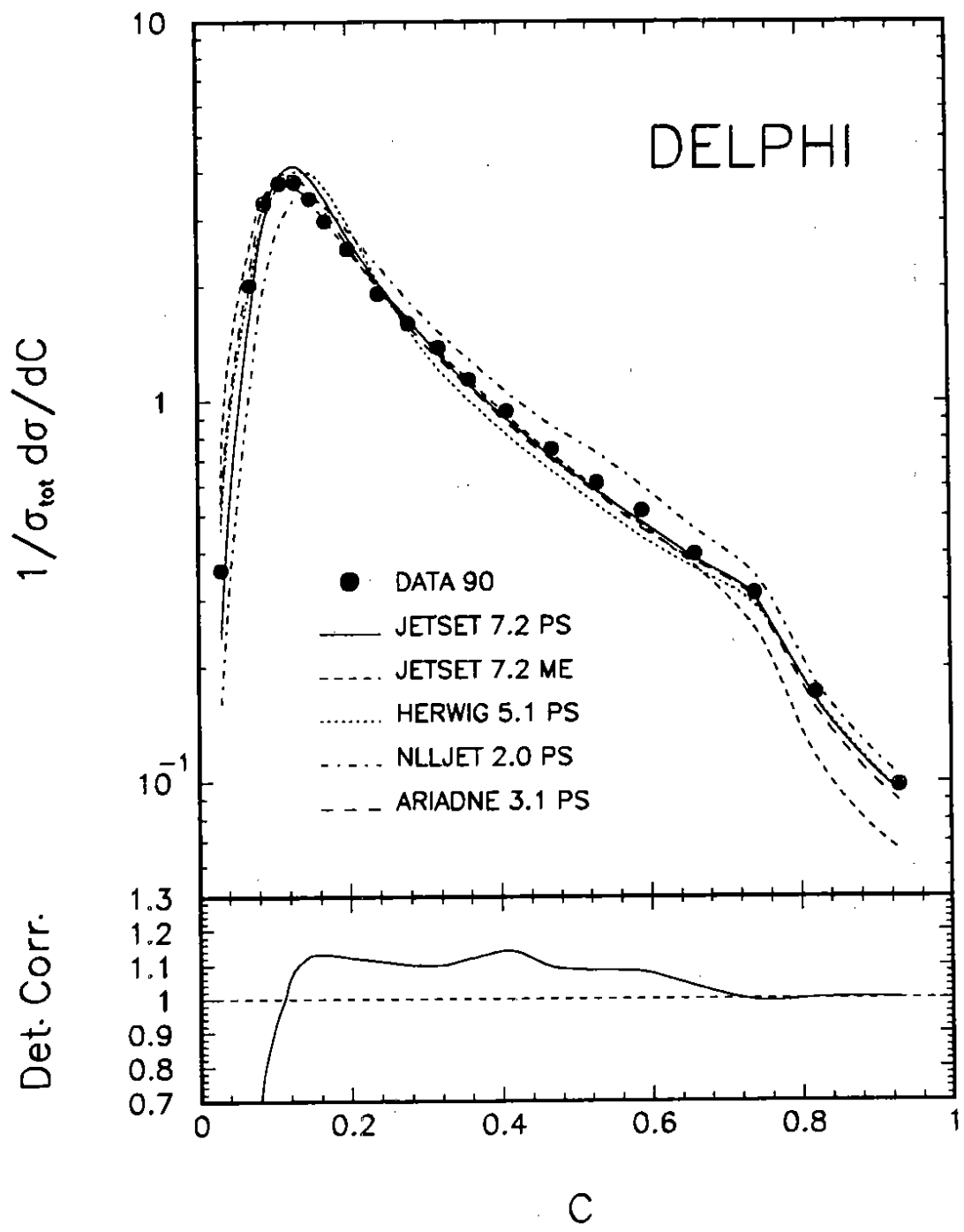
Figure 1a)

figure 1b)

figure 1c)
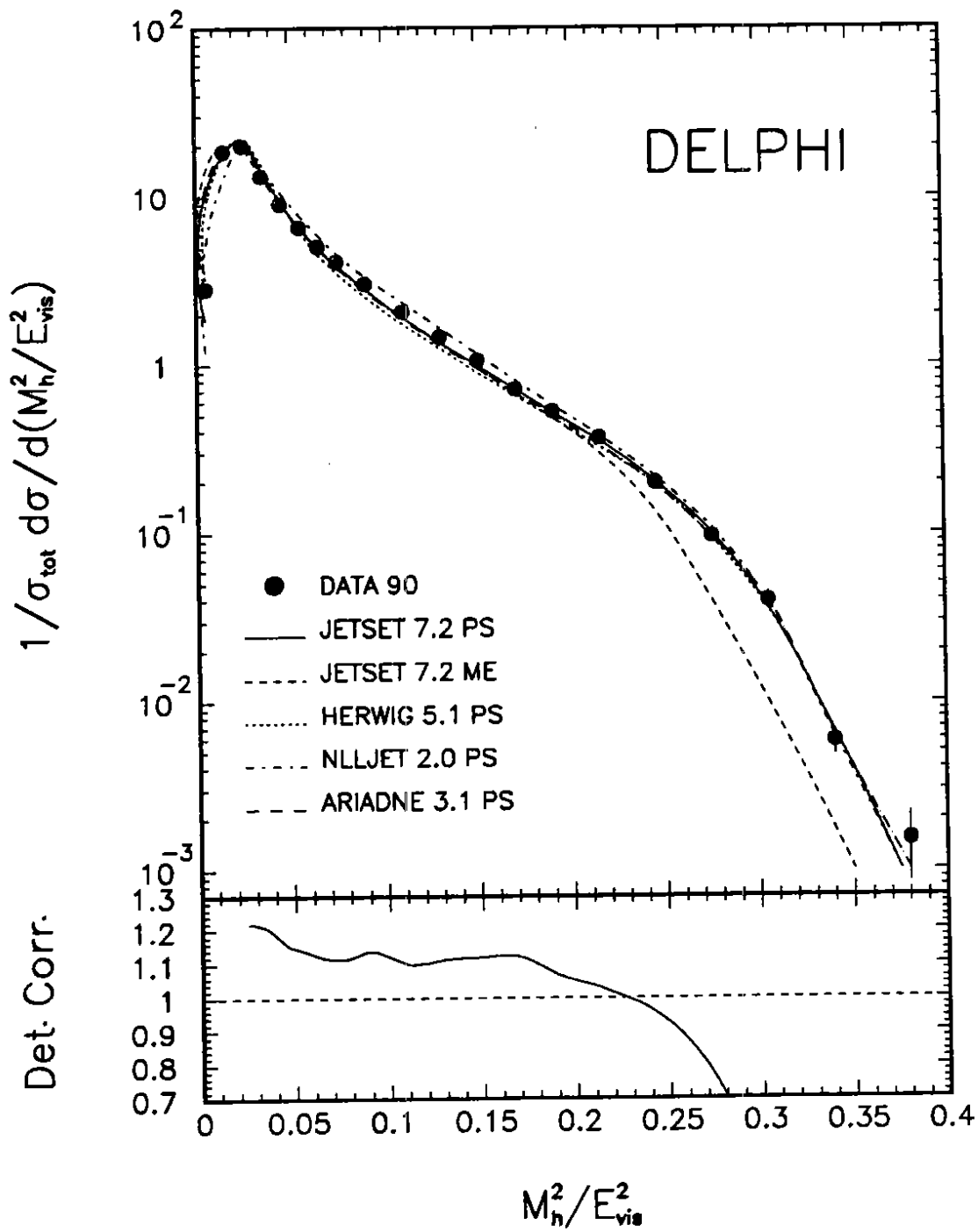
figure 1d)
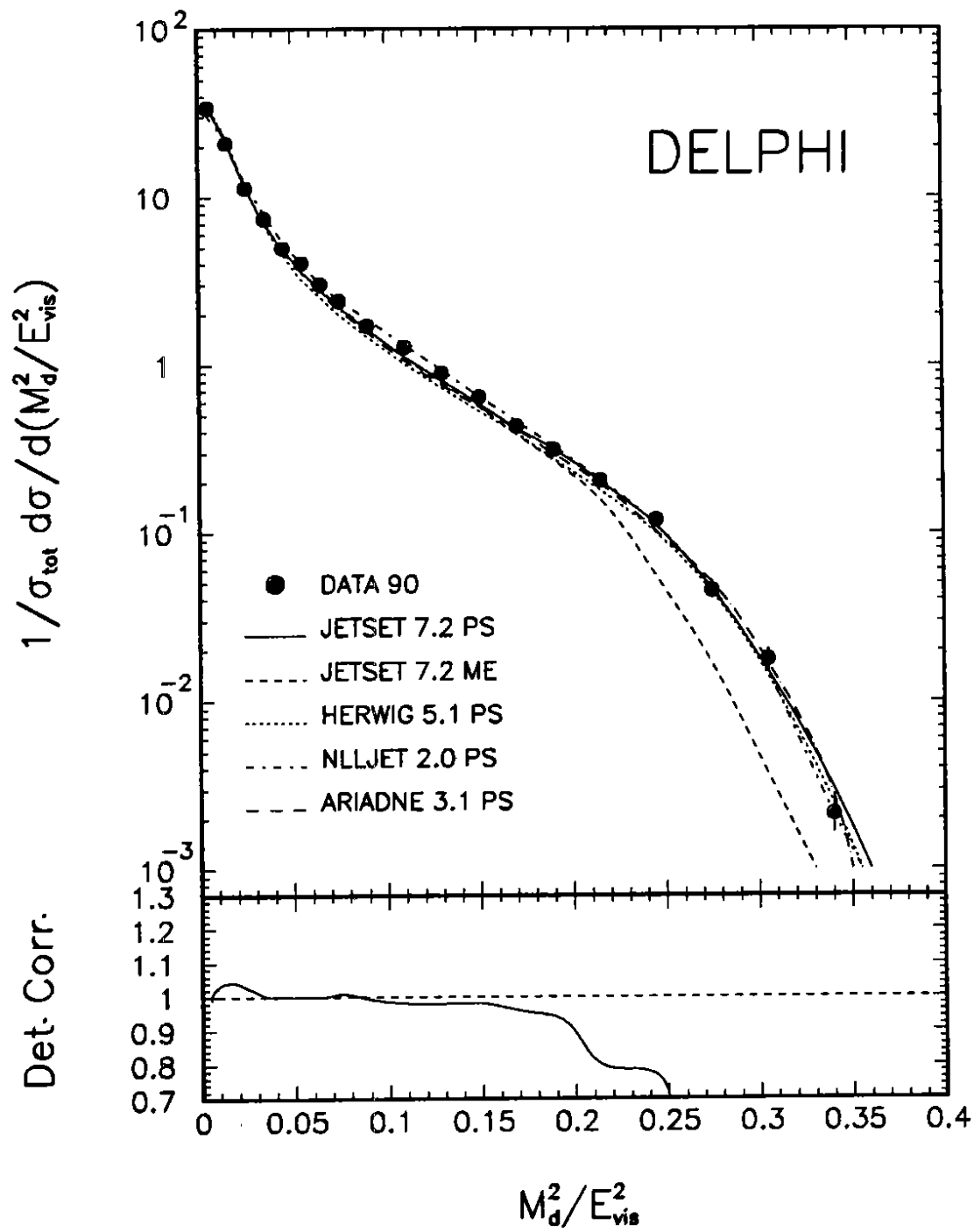
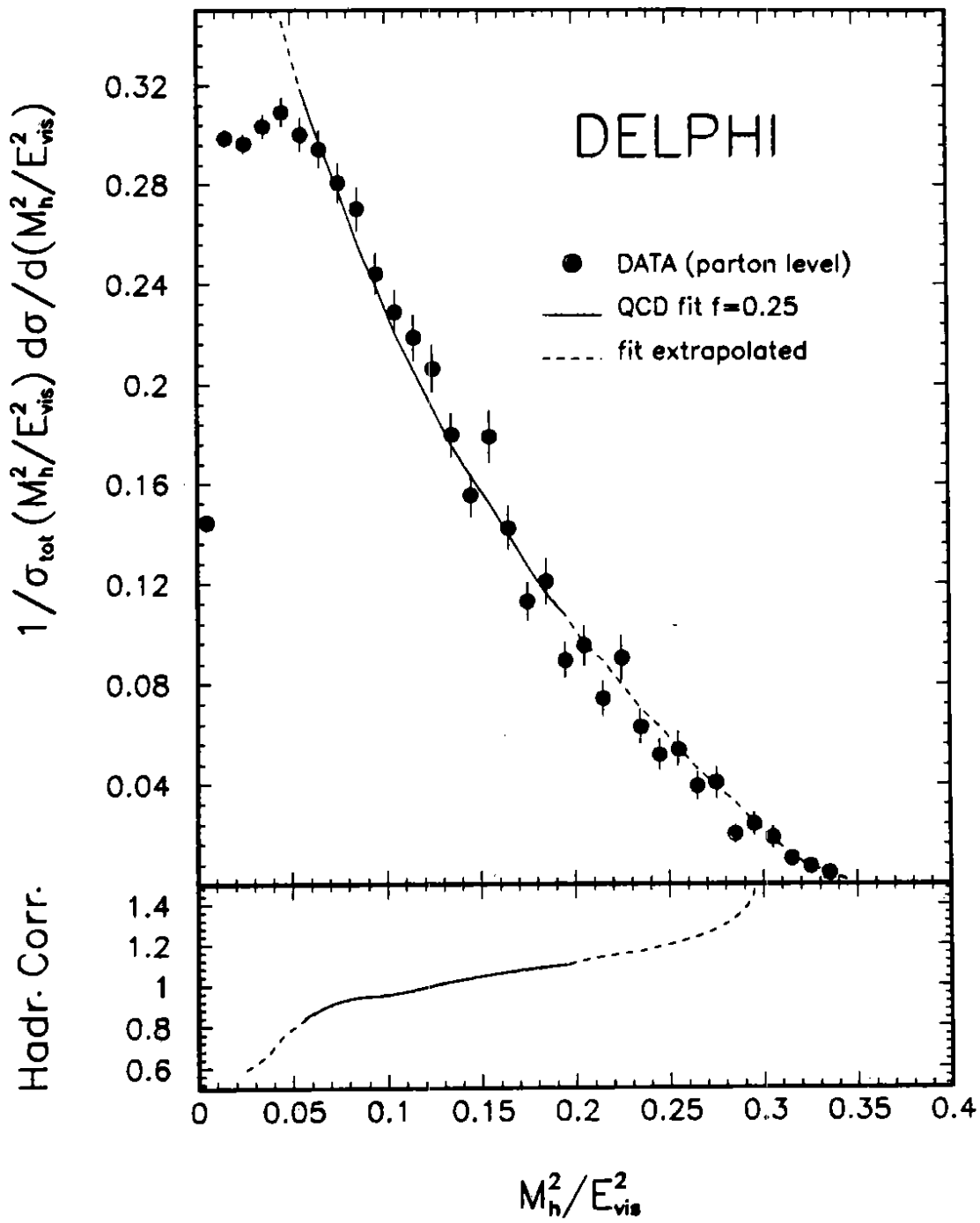figure 1e)
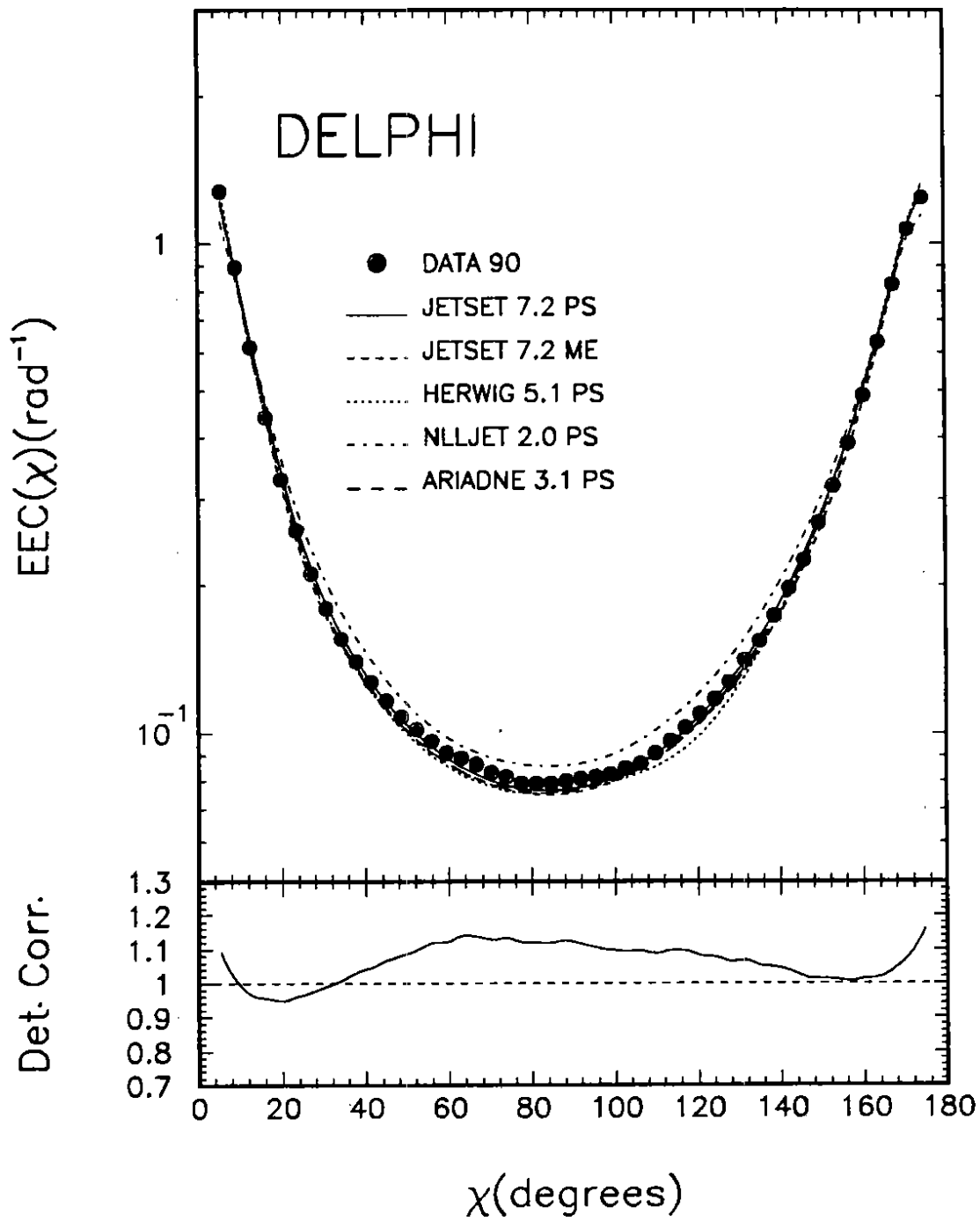
figure 1f)
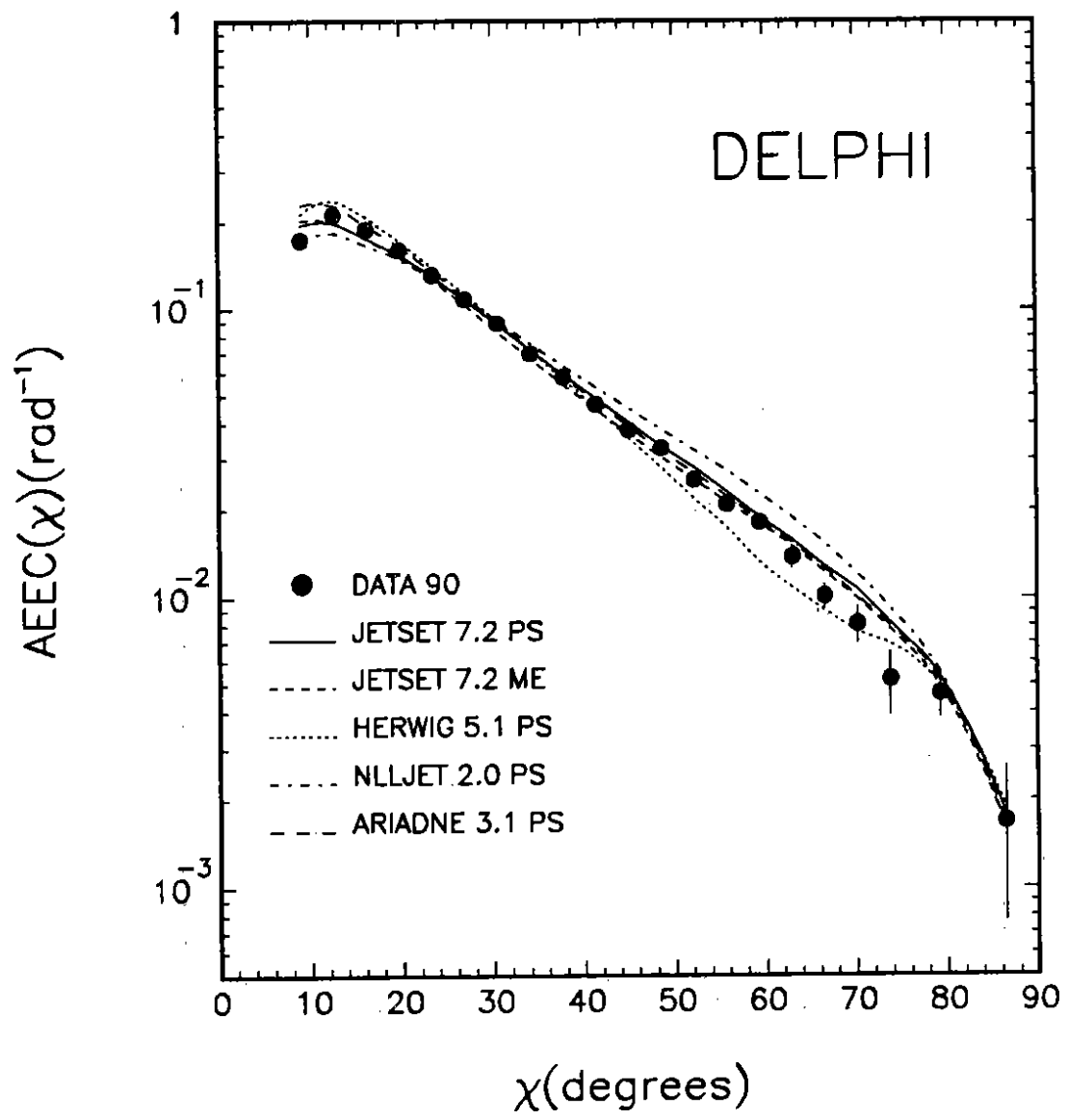
figure 1g)
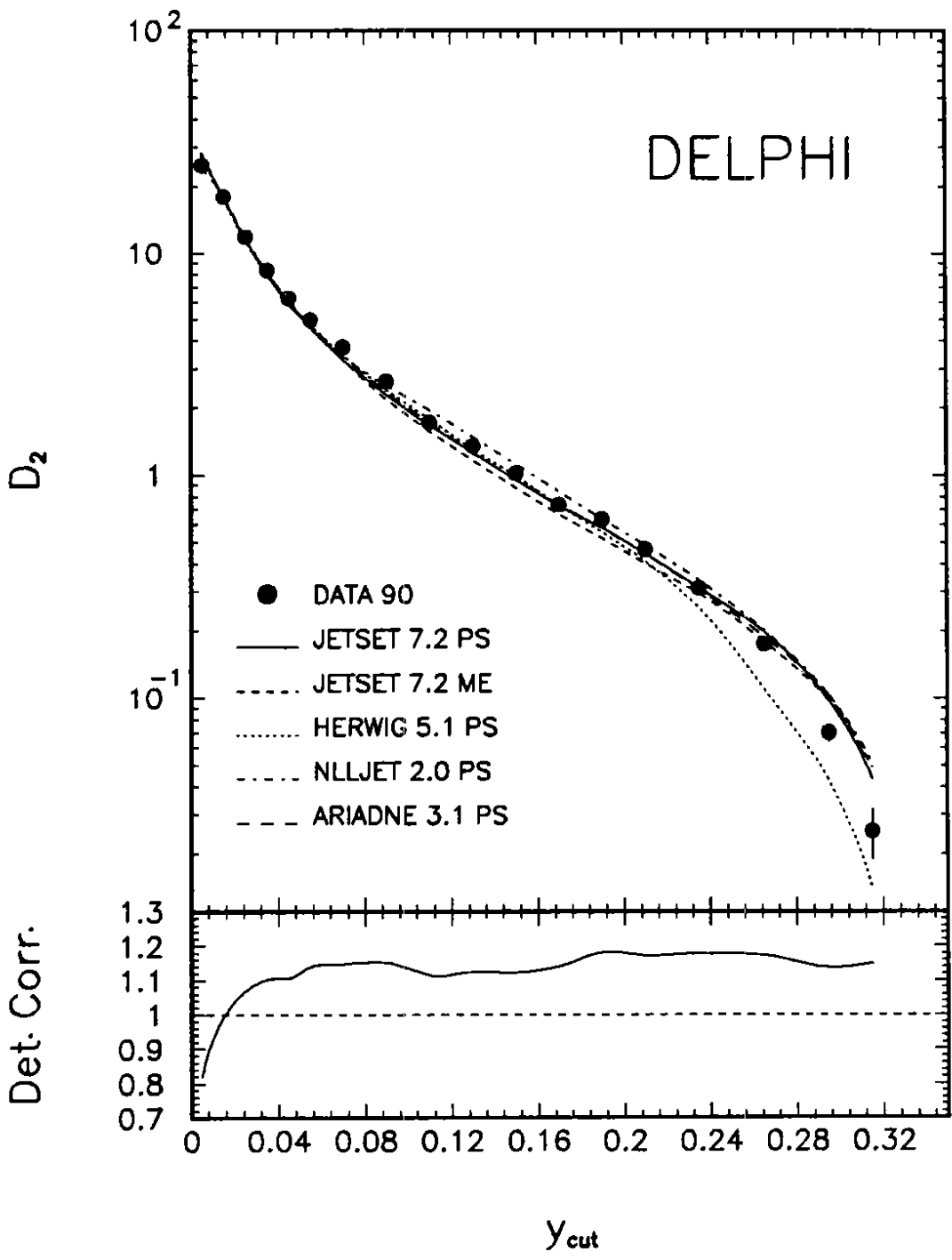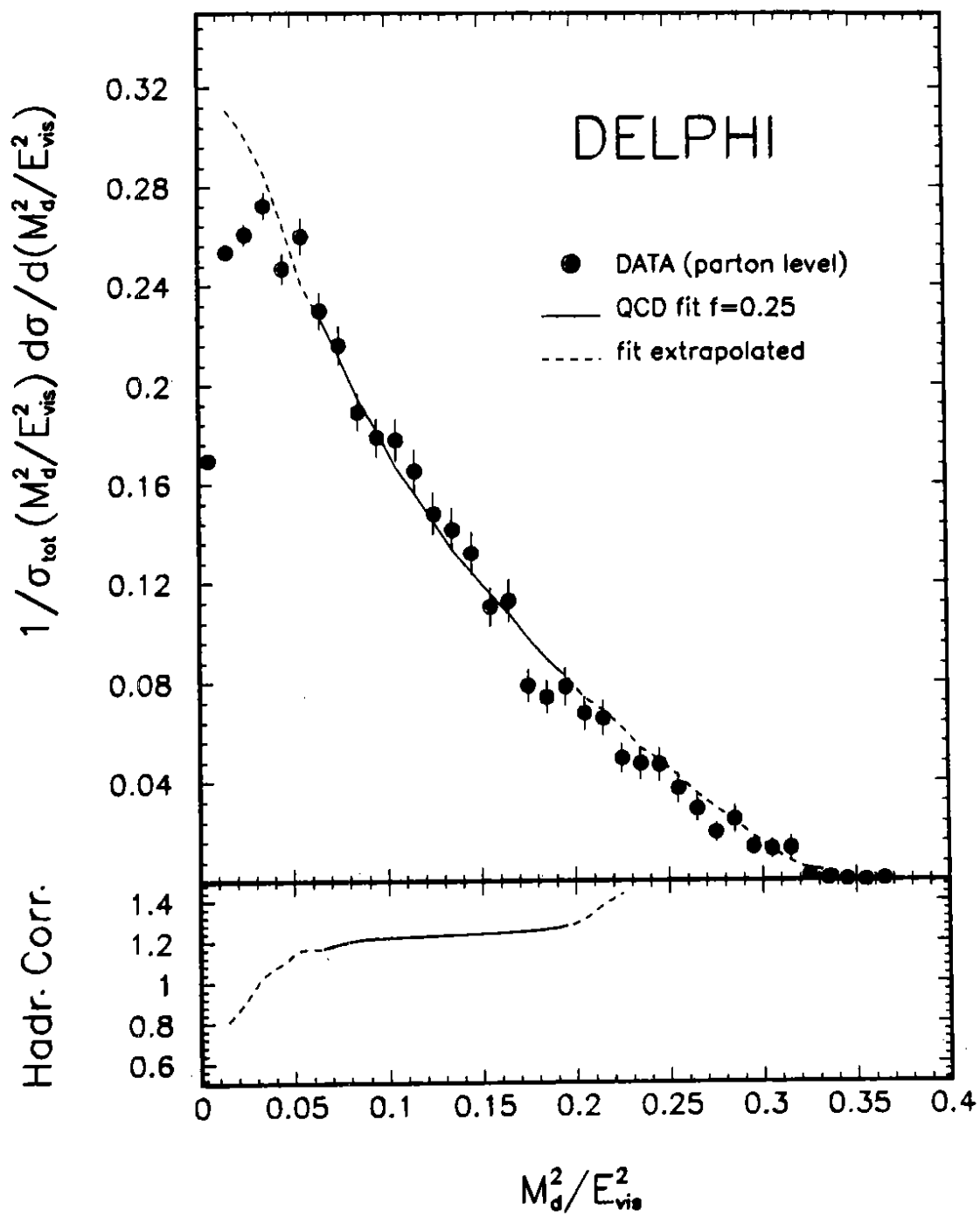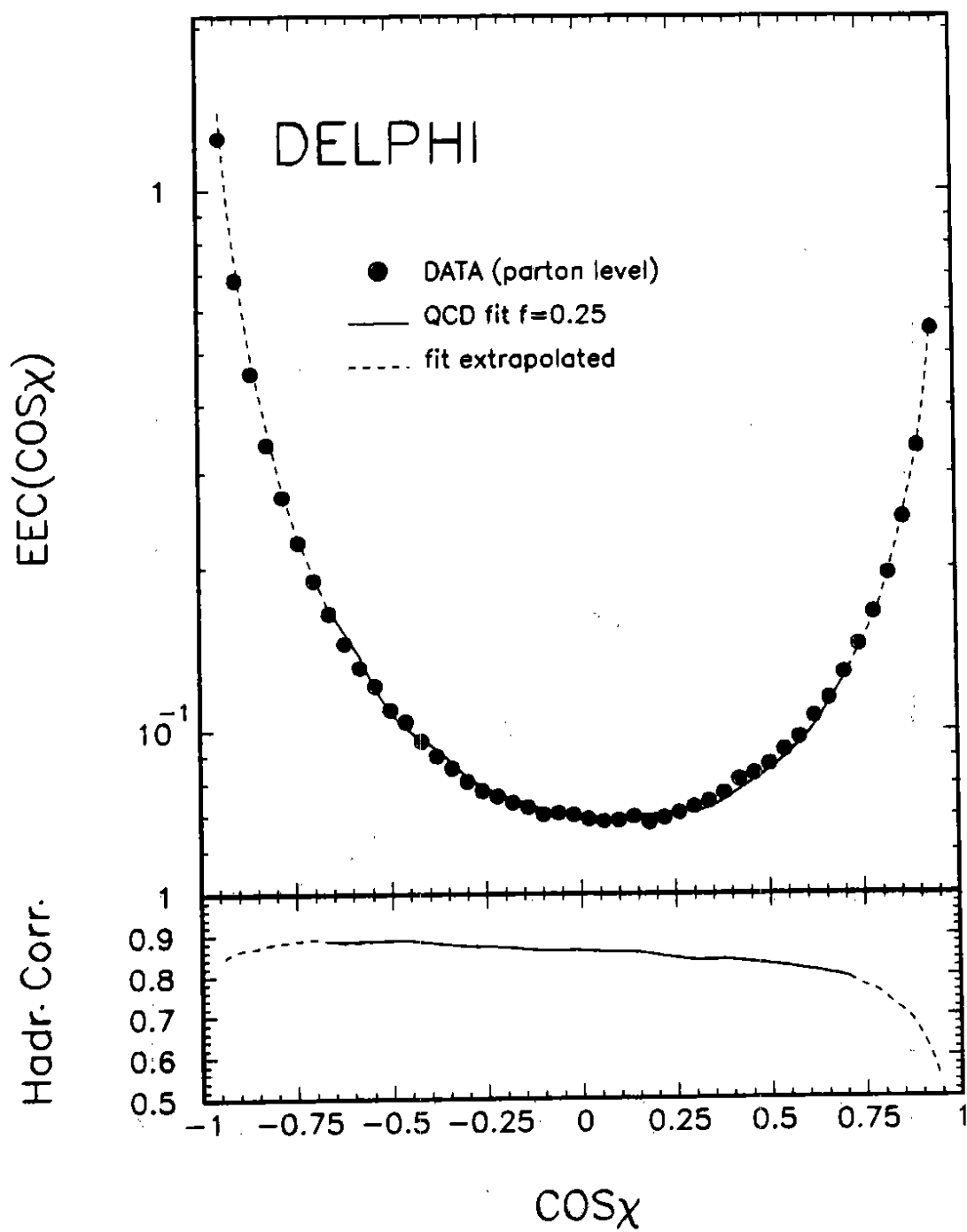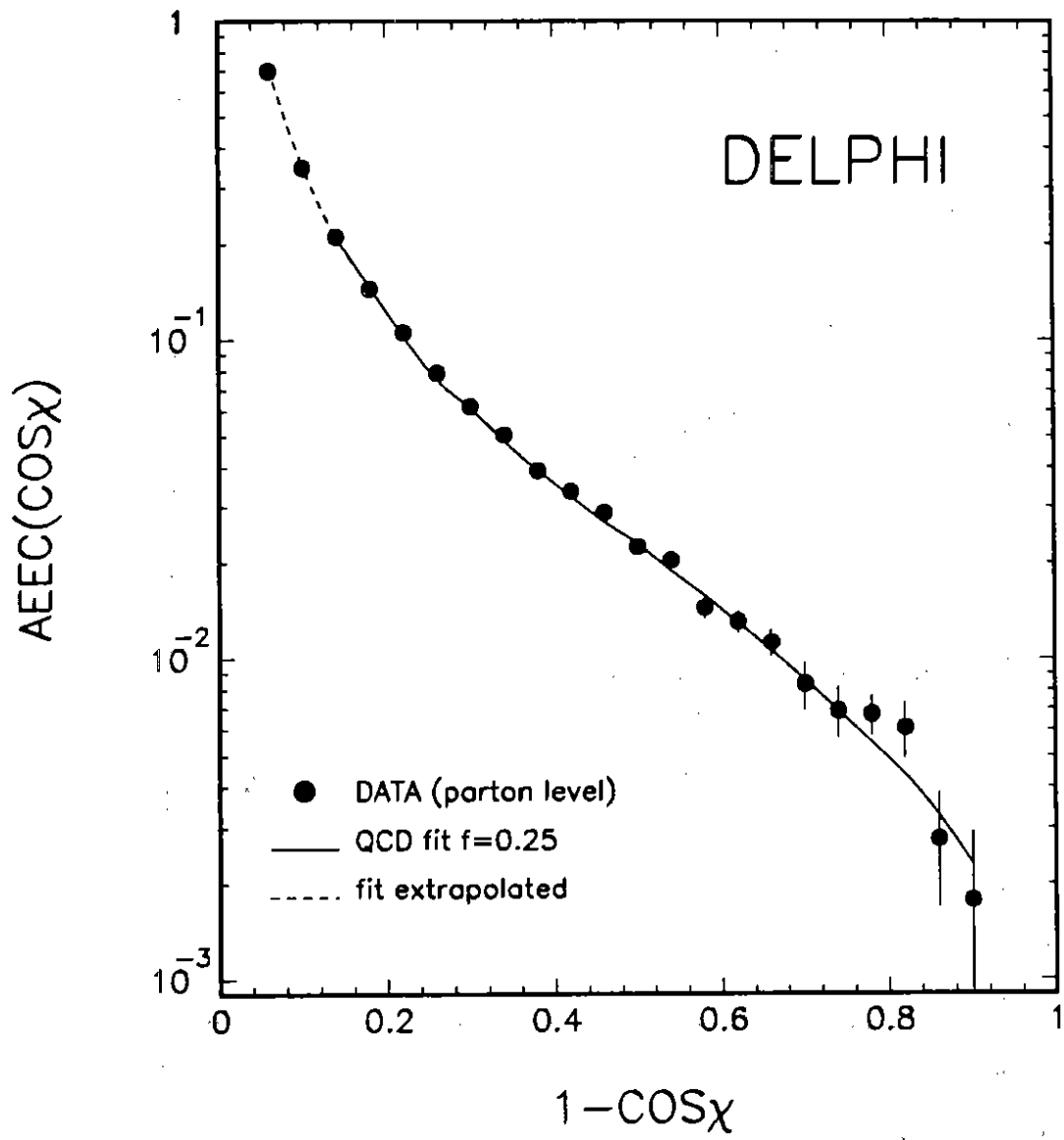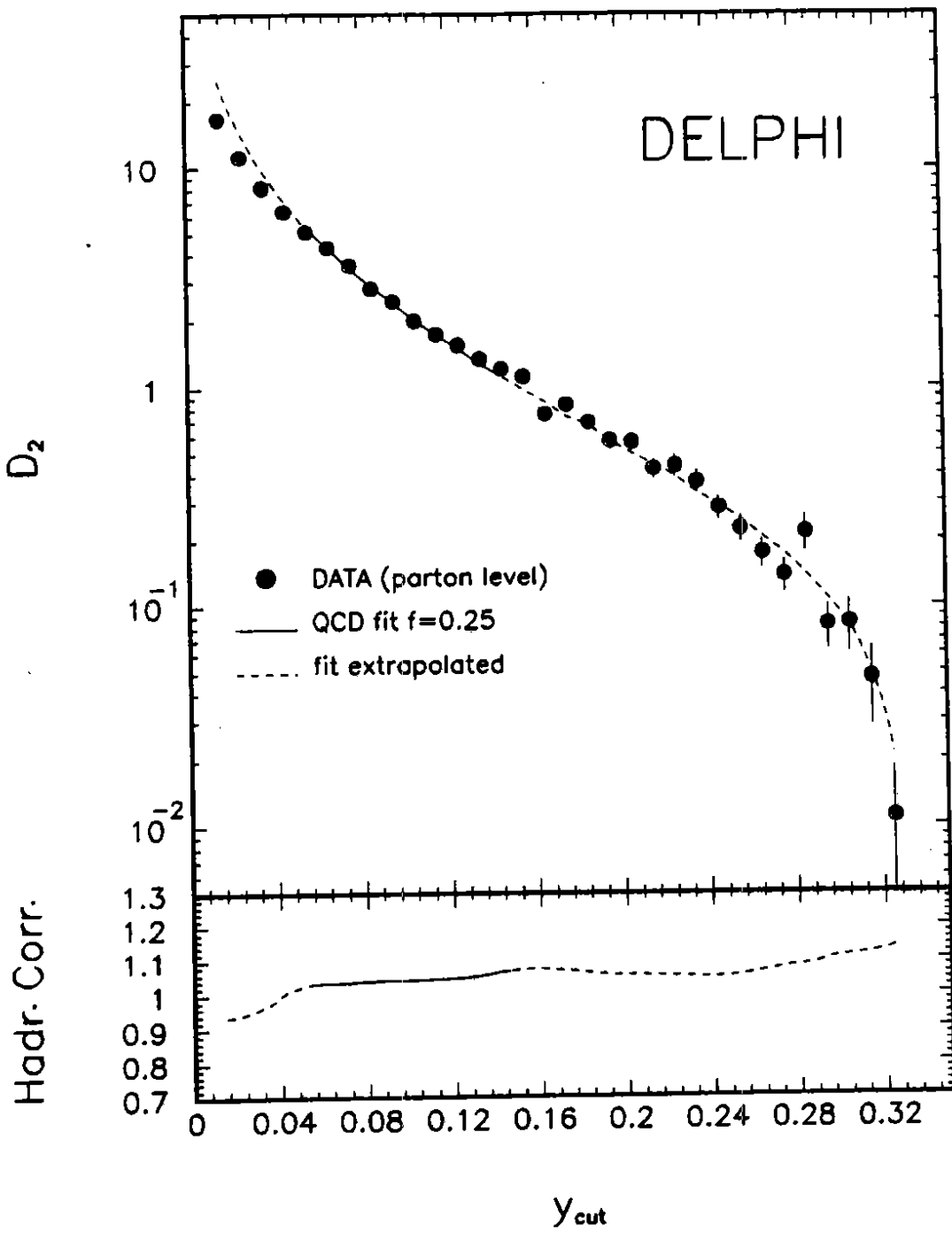
figure 1h)
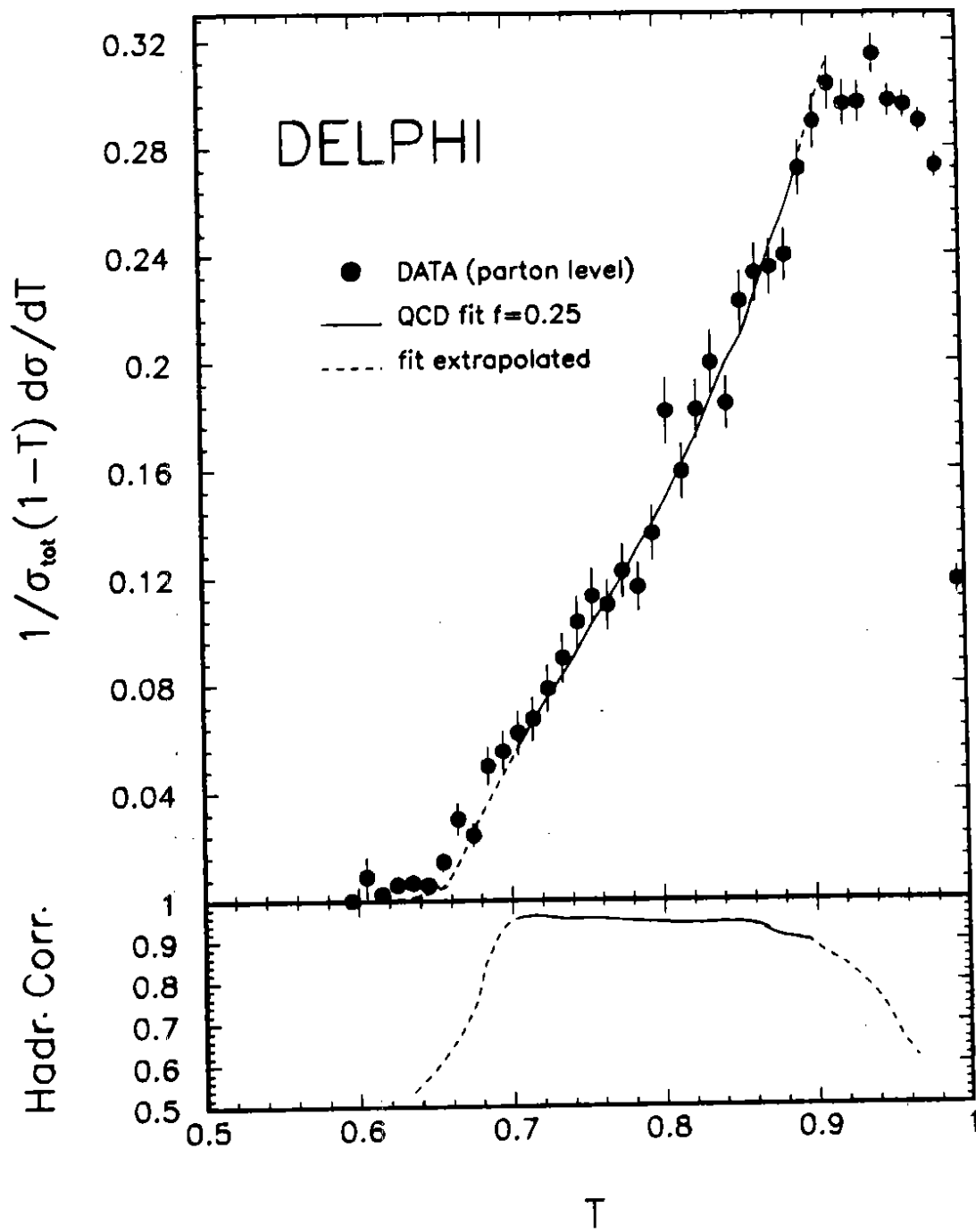
figure 2a)
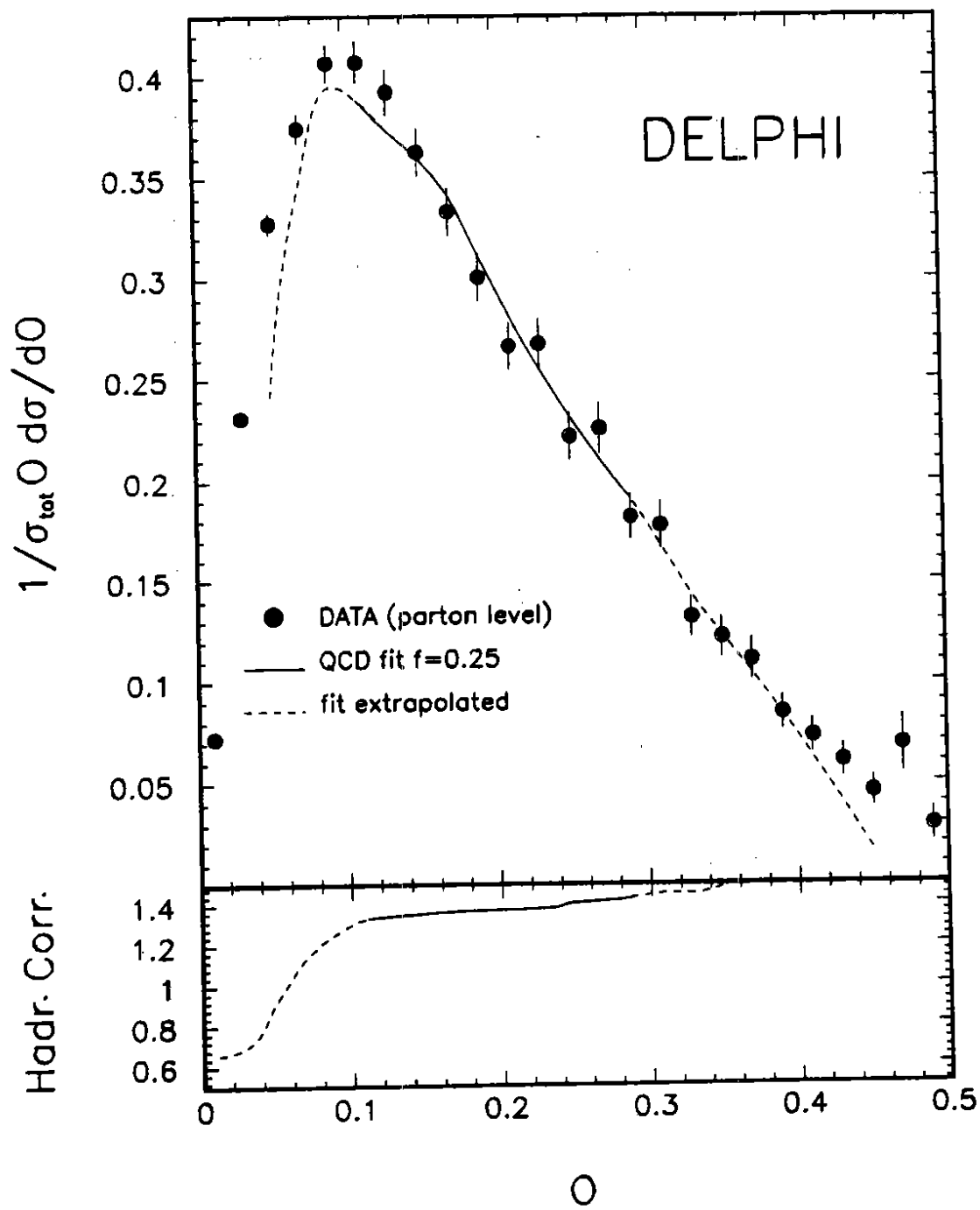
figure 2b)
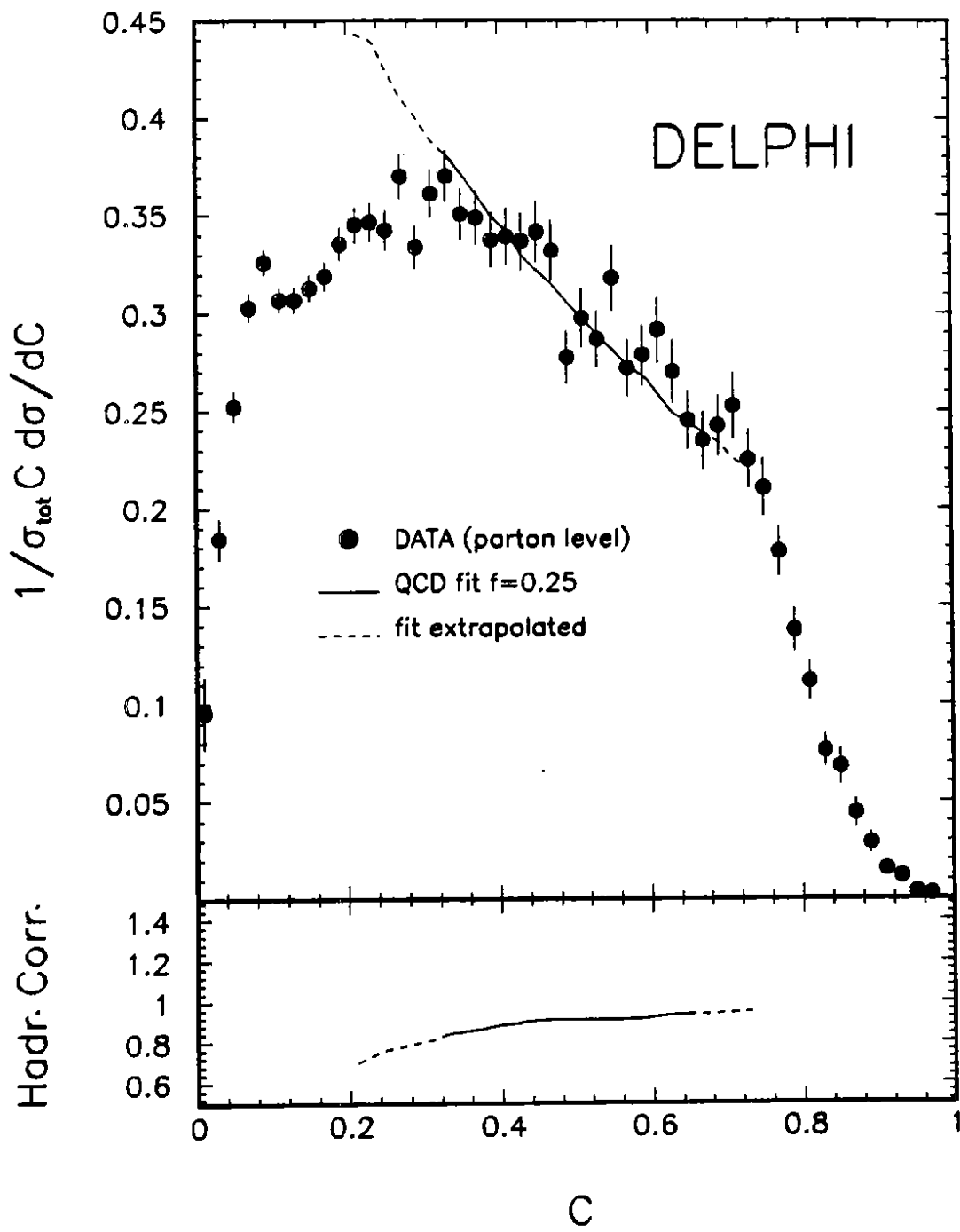
figure 2c)

figure 2d)

figure 2e)

figure 2f)

figure 2g)

figure 2h)

figure 3a)

figure 3b)

figure 4)